DELPHI Collaboration

DELPHI 95-140 PHYS 565
30 August, 1995

Performance of Muon Identification in DELPHI for the 93 and 94 Data

F. Stichelbaut
CERN, PPE division

G.R. Wilkinson
Oxford University

Abstract

The muon identification in the DELPHI muon chambers is performed by the MUCFIX and MUFLAG packages. The improvements obtained in the reconstruction of the Barrel and Forward muon chambers data are presented, together with MC tuning needed to take into account the improved resolution. Muon tagging performance is presented and compared to MC results for the 1993 and 1994 data. Various muon and pion samples coming from leptonic events are used to study the muon identification efficiencies and misidentification probabilities provided by the MUFLAG package.

1 Introduction

The identification of muons produced inside DELPHI is performed through the muon chambers (MUC) that cover most of the 4π solid angle. The association of MUC hits to the trajectory of the charged particles is done inside DELANA with the EMMASS package [1]. By intention the EMMASS fit is general purpose, and is intended as a starting point for all analyses involving muons. The EMMASS fit has very loose criteria of association and a certain fraction of hits will have badly measured coordinates, or will come from nearby background processes. To be able to identify muons produced in a severe environment (such as muons coming from semi–leptonic decay of heavy quarks), the package MUFLAG was developed [2]. This package allows the use of various types of tags, called 'Very Loose', 'Loose', 'Standard' and 'Tight'. These four tags provide to the user different efficiency and purity levels, from very high efficiency but with also large backgrounds to high purity but with lower efficiency. To each of these tags corresponds a specific refit procedure which is intended to reject bad hits. Before this refit, the imperfections of the DELANA processing are cured as much as possible within the MUCFIX package [3].

With the increase of leptonic events statistics available in 1993 and 1994 data, a more precise analysis of the muon chambers behaviour can be achieved and most systematics affecting resolution cured. Selection of new muon samples, such as muons coming from τ decay or produced in two photons collisions, becomes also possible, especially in the DELPHI Forward region. These samples allow the study of the momentum dependence of the muon tagging efficiency.

In section 2 we will briefly recall the main features of muon tagging in DELPHI as it is done inside MUFLAG. The selection of data samples used to study muon identification efficiencies and misidentification probabilities is the subject of section 3. The improvements achieved in the Forward and in the Barrel regions will be described in sections 4 and 5 respectively. The muon identification efficiencies obtained for the 93C and 94B real and MC data are presented in section 6. Finally, the misidentification probabilities corresponding to the various muon tags are discussed in section 7.

2 Muon tagging in DELPHI

The muon tagging done with the MUFLAG package is described in details in reference [2]. In this section, we briefly recall its main features.

All muon chamber information that MUFLAG uses comes originally from EMMASS [1], a module running within the central analysis program DELANA that fits tracks to muon chamber hits. The fit is between the measured coordinates ($R\phi$ and z in the Barrel, x and y in the End Caps) and errors of the muon chamber hit points, and the equivalent coordinates of the extrapolated track, plus direction (Θ and Φ), together with full covariance matrices which take into account the propagated measurement errors and multiple scattering commensurate with a muon of the measured track momentum. The fit information includes a global χ^2 of fit, $\chi^2_{\rm global}$, and a χ^2 expressing the contribution to the fit from the muon chambers themselves, $\chi^2_{\rm muc}$. A extrapolation χ^2, $\chi^2_{\rm ex} \equiv \chi^2_{\rm global} - \chi^2_{\rm muc}$, is also defined to express the contribution to the fit from the extrapolation.

These χ^2's can be used to define a 'good association', and together with the pattern of associated layers, give in principle all information that is needed to select muons in

DELPHI. In practice, the EMMASS fit has very loose criteria of association, and a certain fraction of hits will have badly measured coordinates, or will come from nearby background processes. These pull the fit and dilute the discriminatory power of the χ^2's. Thus it is desirable to drop bad hits and remake the fit without them; the severity of the definition of 'bad hits' depends on the analysis. Furthermore, certain systematic effects will be uncovered by the DELANA processing, both concerning the track extrapolation and the muon chamber information itself. The MUCFIX package [3] allows for the correction of all relevant systematics, and a repeat of the EMMASS fit with cuts set by the user.

The MUFLAG package is used to initialise MUCFIX with different refit options for each tag type. The information provided by the refit is then used to construct tag variables. According to the tag type, cuts on these variables are made for each candidate track. Finally, those passing the cuts are flagged as muons to the user.

We describe the refit options and the variables used for the various muon tags in the forward (MUF) and barrel muon chambers (MUB) separately.

2.1 Muon Tagging in MUF

In the track refit to the MUF information, bad hits are dropped according to a $\chi^2_{\text{bad hit}}$, which is defined:

$$\chi^2_{\text{bad hit}} \equiv \left(\frac{x_{\text{fit}} - x_{\text{muc}}}{\sigma^x_{\text{muc}}}\right)^2 + \left(\frac{y_{\text{fit}} - y_{\text{muc}}}{\sigma^y_{\text{muc}}}\right)^2 \tag{1}$$

where the subscript 'fit' refers to the fitted track, and 'muc' to the muon chamber measurement point. For the Very Loose tag, the cut is made at $\chi^2_{\text{bad hit}} > 1000$. The Loose, Standard and Tight tags use the same refit options, with a cut $\chi^2_{\text{bad hit}} > 10$.

Table 1: Muon Tagging Criteria in MUF

Variable	Very Loose tag	Loose tag	Standard tag	Tight tag
N_{layer}	≥ 1	≥ 1	≥ 1	≥ 1
N_{outer}	No cut	No cut	≥ 1	≥ 1
χ^2_{global} p.d.f.	No cut	≤ 7	≤ 4	≤ 2
χ^2_{ex} p.d.f.	No cut	≤ 7	≤ 3	≤ 1.5

The tracks in the event having been refitted, the χ^2_{global} and $\chi^2_{\text{ex}}$are immediately available. The number of degrees of freedom for the former is twice the number of associated layers. The equivalent quantity for the latter is not well defined; as a working variable we choose to use N_{ex} where:

$$N_{\text{ex}} \equiv \begin{cases} 1 & \text{if number of associated layers} = 1 \\ 2 & \text{if number of associated layers} = 2 \\ 4 & \text{otherwise} \end{cases} \tag{2}$$

The other relevant tagging variables are the total number of associated layers, N_{layer}, and the number of associated hits outside the iron, N_{outer}, in the layers 3 and 4 of MUF.

The muon tagging criteria used in MUF are listed in table 1 for the 4 muon tags.

2.2 Muon Tagging in MUB

In the MUB, the Very Loose, Loose and Standard tags use the same refit options and bad hits are dropped according to the $\chi^2_{\text{bad hit}}$ defined:

$$\chi^2_{\text{bad hit}} \equiv \left(\frac{R\phi_{\text{fit}} - R\phi_{\text{muc}}}{\sigma^{R\phi}_{\text{muc}}} \right)^2 \tag{3}$$

The cut is made at $\chi^2_{\text{bad hit}} > 1000$ for the Very Loose tag and $\chi^2_{\text{bad hit}} > 16$ for the two other tags. Note that this $\chi^2_{\text{bad hit}}$ involves only the azimuthal coordinate. It is related to the presence of more extended tails in the z distribution than in the azimuthal distribution (see below). This emphasis on $R\phi$ is continued into the final cuts, and further χ^2's are constructed in addition to the normal χ^2_{global} and χ^2_{ex}. The extrapolated azimuthal χ^2, $\chi^2_{\text{ex azth}}$, is defined:

$$\chi^2_{\text{ex azth}} \equiv \left(\frac{R\phi_{\text{fit}} - R\phi_{\text{ex}}}{\sigma^{R\phi}_{\text{ex}}} \right)^2 + \left(\frac{\Phi_{\text{fit}} - \Phi_{\text{ex}}}{\sigma^{\Phi}_{\text{ex}}} \right)^2 \tag{4}$$

where the subscript 'ex' refers to the extrapolated track. These quantities are taken at the layer closest to the interaction point. We use $N_{\text{ex}}/2$ as the number of degrees of freedom. Analogously, we form an extrapolated polar χ^2, $\chi^2_{\text{ex polar}}$:

$$\chi^2_{\text{ex polar}} \equiv \left(\frac{z_{\text{fit}} - z_{\text{ex}}}{\sigma^{z}_{\text{ex}}} \right)^2 + \left(\frac{\Theta_{\text{fit}} - \Theta_{\text{ex}}}{\sigma^{\Theta}_{\text{ex}}} \right)^2 \tag{5}$$

also with $N_{\text{ex}}/2$ as the number of degrees of freedom. The total azimuthal χ^2, $\chi^2_{\text{global azth}}$, is defined:

$$\chi^2_{\text{global azth}} \equiv \chi^2_{\text{ex azth}} + \sum \left(\frac{R\phi_{\text{fit}} - R\phi_{\text{muc}}}{\sigma^{R\phi}_{\text{muc}}} \right)^2 \tag{6}$$

where the sum runs over the layers with associated hits. We use the number of associated layers as the number of degrees of freedom. The N_{outer} variable is now defined the number of associated hits belonging to the layers 4 to 7 of MUB.

For the tight tag where emphasis is put on purity, the $\chi^2_{\text{bad hit}}$ is defined:

$$\chi^2_{\text{bad hit}} \equiv \left(\frac{R\phi_{\text{fit}} - R\phi_{\text{muc}}}{\sigma^{R\phi}_{\text{muc}}} \right)^2 + \left(\frac{z_{\text{fit}} - z_{\text{muc}}}{\sigma^{z}_{\text{muc}}} \right)^2 \tag{7}$$

and the cut is made at $\chi^2_{\text{bad hit}} > 10$. No further variable is used in addition to N_{outer} and χ^2_{global}.

These refit conditions and tag variables have been used in MUB for the 93C and the first 94B short DST production (named 94B1). The muon tagging criteria used for these two data sets are shown in table 2.

Since then, a new calibration of MUB delay lines has been achieved, allowing a significant improvement in the z resolution (see section 5). It has then been found possible to include the z measurements in the definition of $\chi^2_{\text{bad hit}}$ for all the tags as it was done before for the Tight tag (see relation (7)). As regards the dropping of bad layers, the cut is made at $\chi^2_{\text{bad hit}} > 1000$ for the Very Loose tag and $\chi^2_{\text{bad hit}} > 7$ for the three other tags. The special χ^2's defined previously are no longer used and the muon tagging is based on the 4 natural variables N_{layer}, N_{outer}, χ^2_{global} and χ^2_{ex}, as it is done in MUF.

These tag variables have been used for the second short DST production of 94B data, named 94B2. The muon tagging criteria used for the 4 tags in MUB are listed in table 3.

Table 2: Muon Tagging Criteria in MUB for 93C and 94B1 Data

Variable	Very Loose tag	Loose tag	Standard tag	Tight tag
N_{layer}	≥ 1	≥ 1	≥ 1	≥ 1
N_{outer}	No cut	No cut	≥ 1	≥ 1
χ^2_{global} p.d.f.	No cut	No cut	No cut	≤ 2.3
$\chi^2_{global\,azth}$ p.d.f.	No cut	≤ 12	≤ 7	No cut
$\chi^2_{ex\,azth}$ p.d.f.	No cut	≤ 12	≤ 8	No cut
$\chi^2_{ex\,polar}$ p.d.f.	No cut	≤ 15	≤ 12	No cut

Table 3: Muon Tagging Criteria in MUB for 94B2 Data

Variable	Very Loose tag	Loose tag	Standard tag	Tight tag
N_{layer}	≥ 1	≥ 1	≥ 1	≥ 1
N_{outer}	No cut	No cut	≥ 1	≥ 1
χ^2_{global} p.d.f.	No cut	≤ 6	≤ 4	≤ 2
χ^2_{ex} p.d.f.	No cut	≤ 5	≤ 3	≤ 1.5

3 Data Samples Selection

To provide a muon sample covering the full momentum range from 3 GeV/c to 45 GeV/c, we use three different channels :

- $Z^0 \rightarrow \mu^+\mu^-$ events, giving a high statistics sample of muons with momentum close to 45 GeV/c;
- $Z^0 \rightarrow \tau^+\tau^-$ events where at least one of the $\tau^- \rightarrow \mu^-\bar{\nu}_\mu\nu_\tau$, providing a continuous spectrum of muon momentum between 3 GeV/c and $\sim$ 40 GeV/c;
- $\gamma\gamma \rightarrow \mu^+\mu^-$ events, giving low momentum muons produced mainly in the Forward region.

To study the misidentification probability (see section 7), we use a pion sample coming from $Z^0 \rightarrow \tau^+\tau^-$ events with a 1 versus 3 charged particles topology, the 3 particles belonging to the same hemisphere coming from the decay $\tau^- \rightarrow \pi^-\pi^-\pi^+\nu_\tau$.

For all the selected events, we ask for a data quality flag between 4 and 7 for MUB and 5 and 7 for MUF.

3.1 Channel $Z^0 \rightarrow \mu^+\mu^-$

The selection of the muon pairs events is mainly based on their kinematical properties. Use is also made of the electromagnetic and hadronic calorimeters to identify the muon candidates and to reject particles faking a muon in one of these two calorimeters. This selection is based on the standard DELPHI $Z^0 \rightarrow \mu^+\mu^-$ analysis.

Only events with exactly two charged particles are considered. Each of these two charged particles must fulfil the following criteria :

- Their momentum must be greater than 20 GeV/c ;
- The impact parameter r with respect to the interaction point must be lower than the quantity r_{max}, where $r_{max} = 0.2$ cm if the charged particle has been detected in the VD, $r_{max} = 1.5$ cm if it has not been seen in the VD but in the ID or in the TPC and $r_{max} = 6.0$ cm in all other cases. These requirements are made to reduce the cosmic background.
- The particle must be identified as a muon candidate, depositing an energy compatible with that of a mip in at least one of the two DELPHI calorimeters. In the electromagnetic calorimeter (HPC or FEMC), the deposited energy must be lower than 1.5 GeV. In the hadronic calorimeter, the mean energy deposition per hit layer of the HCAL, $E_{\rm hlay}$, must remain lower than 5 GeV. Some energy deposition in at least one of the two last layers of the HCAL is also required. The quantity $E_{\rm hlay}$ is obtained after correction of the total energy associated to the charged particle in the HCAL for its polar angle dependence, θ, with the following relation :

$$E_{\rm hlay} = \begin{cases} \frac{E_{\rm HCAL}\,\sin^2\theta}{N_{\rm Hlayers}} & \text{if } 50^\circ \leq \theta \leq 130^\circ \\ \frac{E_{\rm HCAL}}{N_{\rm Hlayers}} & \text{if } \theta < 50^\circ \text{ or } \theta > 130^\circ \end{cases} \quad (8)$$

  where $N_{\rm Hlayers}$ is the number of layers in the HCAL with deposited energy.
- The energy associated to the charged particle in the electromagnetic calorimeter must be lower than 10 GeV and $E_{\rm hlay}$ must remain below 5 GeV.

In addition, the acolinearity of the two muon candidates must be lower than 1°. To further reduce the cosmic background, the quantity $\mid z_1 - z_2 \mid$ must be lower than 4 cm when both tracks have been detected in the TPC, z_i being the longitudinal distance between the point of closest approach of track i and the interaction point.

To study muon tagging, only muon candidates inside the momentum and polar angles acceptance of the muon chambers are used. They must possess a momentum greater than 3 GeV/c and be emitted in the following polar angle intervals :

- $52^\circ < \theta < 88.5^\circ$ or $91.5^\circ < \theta < 128^\circ$ for the Barrel region ;
- $20^\circ < \theta < 42^\circ$ or $138^\circ < \theta < 160^\circ$ for the Forward region.

We restrict our analysis to these θ ranges because of the absence (or only partial coverage) of muon chambers for $42^\circ < \theta < 52^\circ$ ($128^\circ < \theta < 138^\circ$) and because of the poor momentum resolution and track reconstruction for $\theta < 20^\circ$ ($\theta > 160^\circ$). For $Z^0 \to \mu^+\mu^-$ events, we also restrict the study of muon identification efficiency to muons having a momentum between 40 and 50 GeV/c. The table 4 shows the final numbers of muon candidates selected in the Barrel and Forward regions for the 93C and 94B real data.

3.2 Channel $\tau^- \to \mu^-\bar{\nu}_\mu\nu_\tau$

The selection of the $\tau^- \to \mu^-\bar{\nu}_\mu\nu_\tau$ events is done in two steps. First, a general $Z^0 \to \tau^+\tau^-$ event selection is applied. This selection relies on standard criteria used by the DELPHI $Z^0 \to \tau^+\tau^-$ analysis in the Barrel region [4]. These criteria are slightly modified to select

Table 4: Muon and Pion Candidates in MUC for the 93C and 94B Data

Sample	Year	Barrel	Forward
$Z^0 \rightarrow \mu^+\mu^-$	93C	20964	7323
	94B	46852	17407
$\tau^- \rightarrow \mu^-\bar{\nu}_\mu\nu_\tau$	93C	3828	1520
	94B	8265	3394
$\gamma\gamma \rightarrow \mu^+\mu^-$	93C	703	2338
	94B	945	3054
$\tau^- \rightarrow \pi^-\pi^-\pi^+\nu_\tau$	93C	6093	1155
	94B	11945	2196

τ pairs in the Forward region [5]. Secondly, events containing a muon candidate are selected using only the hadron calorimeter informations.

To define a $Z^0 \rightarrow \tau^+\tau^-$ event, the following criteria are used :

- $N_{prong} \leq 12$, N_{prong} being the total number of reconstructed charged particles in the event.
- $2 \leq N_{trk} \leq 6$ where N_{trk} is the number of charged particles coming from the interaction region ($| r |< 5$ cm and $| z |< 10$ cm) and with a track length greater than 30 cm.
- At least one charged particle in each hemisphere defined by the plane perpendicular to the event thrust axis. In case of more than one particle in a given hemisphere, the most energetic one is defined as the leading one. When both leading tracks have a polar angle outside of the Barrel region ($43° < \theta < 137°$), the event is said to be produced in the Forward region.
- For events produced in the Barrel, the two leading tracks must satisfy the following impact parameter cuts : $| r | < 1.5$ cm and $|z| < 5.0$ cm. These two cuts are relaxed to 10 cm in case of a forward event.
- For events produced in the Forward region, a minimal acolinearity angle between the two leading tracks, θ_{acol}, of 1° is required.
- $\theta_{iso} \geq 160°$, θ_{iso} being the minimum angle between two charged particles in opposite hemispheres.
- $E_{vis} > 8$ GeV where E_{vis} is the sum of charged particles momenta and neutral electromagnetic energies.
- $P_{rad} = \sqrt{P_1 + P_2}/E_{beam} < 1.2$ where P_1 and P_2 are the momentum of the two leading tracks and E_{beam} is the beam energy.
- $E_{rad} = \sqrt{E_1 + E_2}/E_{beam} < 1.0$ where E_1 and E_2 are the electromagnetic energy assigned to the two leading tracks, computed by adding all deposited electromagnetic energy inside a cone of 30° (half opening angle) around the charged particle trajectory.

- For events containing only two charged particles, additional cuts are applied to reduce background coming from two-prongs events :

  1. $\mid z_1 - z_2 \mid \leq 3$ cm ;
  2. $\theta_{\rm acol} \geq 0.5°$;
  3. $\mid \vec{P_T} \mid > 0.4$ GeV, where $\vec{P_T}$ is the transverse component of the total momentum of the event;

  for events produced in the Barrel region, and

  1. $\mid z_1 - z_2 \mid \leq 5$ cm ;
  2. $\mid \vec{P_T} \mid > 0.4$ GeV ;

  for events produced in the Forward region.

The $\tau^- \rightarrow \mu^- \bar{\nu}_\mu \nu_\tau$ events are finally selected by requiring that the event contains at least one hemisphere with a single charged particle identified as a muon in the HCAL using the PXHAID tight tag. The event is rejected if $E_{\rm hlay}$ is greater than 5 GeV or if the electromagnetic energy associated to the charged particle is greater than 5 GeV.

Figure 1 shows the polar angle and the momentum distributions of the muon candidates obtained after applying this selection on the 93C real and MC data. Only the muons satisfying the acceptance cuts of the muon chambers are represented. The contribution of the various background sources is also shown. The contamination of muon candidates by other particles (mainly charged pions) is estimated to be 1.7 ± 0.1 % in the Barrel region and 2.8 ± 0.2 % in the Forward region. The table 4 shows the number of muon candidates selected on the 93C and 94B data.

3.3 Channel $\gamma\gamma \rightarrow \mu^+\mu^-$

To select the $\gamma\gamma \rightarrow \mu^+\mu^-$ sample, we only consider events containing exactly two charged particles with opposite charge. In addition, these particles must satisfy the following quality criteria : a track length greater than 30 cm, impact parameters $\mid r \mid < 4$ cm and $\mid z \mid < 10$ cm, and a relative momentum error dP/P ≤ 1. The momentum of these two particles must be between 1 and 20 GeV/c. Moreover, the scalar sum of the two momenta must remain lower than 20 GeV/c.

After these simple cuts, the selection of $\gamma\gamma \rightarrow \mu^+\mu^-$ events differs following that the two scattered electrons remain in the beam pipe or at least one is detected in one of the two luminosity detectors (SAT and VSAT for 93 data, STIC and VSAT for 94 data). If no energy is deposited in any of these two luminometers, the event is said "antitagged". We then require that $\mid \cos\theta_1 + \cos\theta_2 \mid \geq 0.2$ to reduce the background coming from colinear two prongs events. The total neutral energy deposited in the HPC and the FEMC must also be lower than 6 GeV. If an energy of at least 20 GeV is detected in either SAT/STIC or VSAT, the event is said "tagged". We then simply ask for a total neutral energy in the electromagnetic calorimeters lower than 5 GeV.

For both "tagged" and "antitagged" events, at least one particle must be identified as muon in the HCAL, using the PXHAID tight tag, or in the MUC, with at least one associated hit.

As the muon chambers information is used to select these events, a special selection of muon candidates has to be used in order not to bias the efficiency study. The two muon candidates are ordered at random. If the first particle is within the acceptance of MUC, it will later be used as muon candidate only if the second particle is identified as muon in the HCAL or in the MUC. If it is not identified as a muon, the entire event is rejected. If the first particle does not satisfy the MUC acceptance cuts, the same procedure is applied on the second particle. This ensures an unbiased sample of muon candidates.

Figure 2 shows the polar angle and momentum distributions of the final muon candidates for the 93C real and MC data. Good agreement between data and MC is obtained. One observes that the muons coming from two-photons collisions are mainly produced in the Forward region. Their momentum is strongly peaked to low values, with a mean value of 4.8 GeV/c. The number of muon candidates selected for the 93C and 94B data are shown in table 4.

3.4 Channel $\tau^- \to \pi^-\pi^-\pi^+\nu_\tau$

As for the $\tau^- \to \mu^-\bar{\nu}_\mu\nu_\tau$ events, the selection of $\tau^- \to \pi^-\pi^-\pi^+\nu_\tau$ events is done in two steps. The first step consists of a general $Z^0 \to \tau^+\tau^-$ selection, as described in section 3.2. Then, only events with a one versus three charged particles topology are considered. The most severe background to this channel is when a single charged particle is produced in a hemisphere together with a photon converting to an electron pair. The following criteria are used in order to select a pion sample with a high purity :

- The total electromagnetic energy deposited in HPC and FEMC must be below 55 GeV and 30 GeV for events produced in the Barrel and Forward region respectively. For forward events, the total electromagnetic energy deposited in the 3 prongs hemisphere must also remain lower than 20 GeV.

- The scalar sum of the momenta of the three charged pions must be greater than 10 GeV/c for barrel events and 16 GeV/c for forward events.

- To remove most of the events containing an electron pair coming from photon conversion, the number of charged particles belonging to the $3\,\pi^{\pm}$ hemisphere and detected in the VD must be at least equal to two. Unfortunately, this criterion can not be used for forward events. We then ask that at least two of the three pions satisfy the cuts $\mid z_{\rm first} \mid < 50$ cm and $\mid R_{\rm first} \mid < 30$ cm, where $z_{\rm first}$ and $R_{\rm first}$ are the z and R coordinates of the first measured point along the charged particle trajectory.

- The $3\,\pi^{\pm}$ invariant mass, $M_{3\pi}$, must be below 2 GeV/c^2 for barrel events and between 0.8 and 1.6 GeV/c^2 for forward events.

- To further reduce the contamination of electron pairs coming from γ conversion, the dE/dx measurements of the TPC are used. Events containing at least one electron candidate are rejected, an electron candidate being defined as a particle with a momentum lower than 6 GeV/c, at least 30 wires with an ionisation measurement in the TPC, a pull value $\mid \Pi^e_{dE/dx} \mid < 2$ for the electron hypothesis and a pull value $\Pi^\pi_{dE/dx} > 2$ for the pion hypothesis.

Figure 3 shows the polar angle and momentum distributions of the pion candidates obtained by applying this selection on the 94B real and MC data. Only the pions satisfying the acceptance cuts of the muon chambers are represented. The particles coming from τ which do not decay into three charged pions are also shown. They are mainly produced by τ decaying into a charged pion and at least one π^0. Within the acceptance of the MUC, they represent 4.21 ± 0.14 % of the pion sample in the Barrel region and 3.1 ± 0.3 % in the Forward region. Other backgrounds, such as $Z^0 \rightarrow e^+e^-\gamma$ events where the photon converts to an electron pair, remain below 1 %. The contamination of muons in the pion sample is considered as negligeable, being lower than 0.1 %. The table 4 shows the number of pion candidates selected on the 93C and 94B data for the two regions.

4 Improvements in the Forward Region

In the MUCFIX note [3], some corrections needed to cure systematic effects in the Forward region were introduced. With the increased statistics in forward muons, new corrections are found to be necessary. They mainly affect the real data and allow for an improvement in the resolution of the forward muon chambers. These corrections are the following :

1. **Delay Line Prepulses.**
   Inside DELANA, the MUF impact points are reconstructed by looking for triplets of time (T_a,T_1,T_2), T_a being the anode time, T_1 and T_2 the propagation times of delay line pulse to both ends. The impact point coordinate along the delay line is then reconstructed using the relation :

   $$y = L/2 + V_{\rm dl}(T_1 - T_2)/2 \tag{9}$$

   where L is the total active length of the delay line (L ~435 cm) and $V_{\rm dl}$ is the delay line pulse propagation velocity ($V_{\rm dl} \sim 0.17$ cm/ns). It appears that the times T_1 or T_2 are sometimes shorter than expected, by an amount between 25 and 50 ns. Studies done on parallel muon data [6] have shown that these shorter times are related to the presence of a small prepulse. This prepulse, moving faster along the delay line than the main one, leads to shorter propagation times if its amplitude is larger than the discrimination threshold. This prepulse is generally detected on only one end of the delay line, the one closest of the production point. This leads to reconstructed y coordinates shifted by ~2 to ~4 cm with respect to the true ones. This prepulse phenomenon affects about 8 % of hits and seems to be related to a too high anode voltage for some MUF layers. To correct for these prepulses, the algorithm used inside DELANA to reconstruct the y coordinate has been modified. To detect the presence of a prepulse, one checks if the quantity

   $$T_{\rm sum} = T_1 + T_2 - \frac{L}{V_{\rm dl}} \tag{10}$$

   is between -50 and -25 ns (this quantity must be close to zero for normal pulses). In this case, the y coordinate is reconstructed using only one propagation time T_1 or T_2 (the longest one, less affected by the prepulse) instead of the time difference. This correction is done automatically inside DELANA starting with the 93C processing. We will later describe its effect on the residual distributions.

2. **Drift Time to Distance Parametrisation.**
   The drift time to distance parametrisation used in DELANA does not describe correctly the true relation. Analysing the parallel muon data, a better description of this relationship can be obtained. The effect of this correction on the 93C muon pairs data is shown in figure 4a. With the corrected relationship, the systematic differences between the measured and the predicted coordinate along the drift axis remain below 1 mm for drift distances lower than 8 cm. They become greater with larger drift distances because of the non–linearity of the drift field close to the chamber edges. This correction is done inside MUCFIX by setting the switch ISTEER(14) to 1. It will be introduced in DELANA for the future reprocessings.

3. **Delay Line Velocities.**
   In principle, the delay lines velocities are stable in time. Nevertheless, the analysis of parallel muon data shows some slight deviations of these velocities with respect to the ones in the DELPHI database. These shifts are corrected within MUCFIX when ISTEER(15)=1. Reduction of systematic differences between the measured and expected coordinates along the delay lines can be observed after this correction (figure 4b).

The effect of these various fixings on the muon chambers resolution is illustrated in figure 5. The figures 5a and 5b show the difference between the coordinate predicted by the charged track extrapolation and the measured one, with the latter obtained from the drift distance or from a delay line respectively. These distributions are obtained from muon pairs coming from Z^0 decays and corresponding to the 93B data without any fixing. The figures 5c and 5d show the same distributions obtained with the 93C data after all fixings have been applied. One clearly sees on figure 5b the presence of large non-Gaussian tails coming from the prepulse effect. These tails have almost disappeared for the 93C data (figure 5d). The use of new calibration constants allows an improvement in the muon chambers resolution. This is demonstrated by the smaller widths obtained with a Gaussian fit to the 93C residual distributions.

The intrinsic resolution of the muon chambers can not be extracted easily from these widths because of the errors affecting the extrapolated coordinates and coming from the multiple scattering. To obtain this resolution, a method relying only on the measured coordinates inside muon chambers is used [6]. Using the measured coordinates of two impact points detected in two parallel quadrants, the muon trajectory is calculated with the hypothesis of a straight line. The impact point coordinates in the two remaining layers are then calculated and compared to the measured ones. A Gaussian fit to these residual distributions gives an intrinsic resolution of 5 mm for the 93B data (no fixing) and 3.5 mm for the 93C data after all fixings.

This intrinsic resolution does not include the systematic errors arising from quadrant misalignment or muon trajectory reconstruction. The study of systematic differences between measured and extrapolated coordinates along DELPHI axis shows strong variations in function of the ϕ angle of the muon (figure 6). The origin of these variations has not yet been clearly understood. The modification of the residual behaviour for $\phi = 90°, 180°, 270°$ and $360°$ seems to indicate that they are related to quadrant position. Rotation of quadrants by a few milliradians around the Z axis allows moreover the variations in some quadrants to be corrected, but not in all of them. The fact that these variations follow similar pattern in the inner and outer quadrants but are amplified in the

later ones tends to indicate a problem related to the muon trajectory reconstruction. As this effect is not well understood, we decided not to correct for it but to slightly degrade the MUF chambers resolution. These systematic variations being larger in End Cap C than in A, it is then necessary to use different resolution in the two End Caps : $\sigma = 3.75$ mm in A and $\sigma = 4.25$ mm in C. These resolutions lead to flat distributions for the global χ^2 probability in both End Caps.

The improvement of the muon chambers resolution has also some implications on the MC data. As previously described in section 2, the global χ^2 is the sum of two contributions : the muon χ^2, $\chi^2_{\rm muc}$, expressing the contribution to the fit from the muon chambers themselves, and the extrapolation χ^2, $\chi^2_{\rm ex}$, expressing the contribution from the extrapolation. In figure 7, the relative weigth of $\chi^2_{\rm ex}$ in the global χ^2 is compared between real and MC data for the three muon samples. It shows that $\chi^2_{\rm ex}$ gives generally a lower contribution to $\chi^2_{\rm global}$ in the MC than in the real data. The explanation of this effect has to be found in the different MUF chambers resolution for the real ($\sigma \sim 4$mm) and simulated data ($\sigma = 5$mm) : with better resolution, the fitted muon trajectory has a tendency to be closer to the measured points and the $\chi^2_{\rm ex}$ will thus increase. To correct for this effect, it is necessary to increase the $\chi^2_{\rm ex}$ value for MC data but leaving unchanged the $\chi^2_{\rm muc}$ value. This is done by scaling the quantities $\Delta T1_{\rm ex}$, $\Delta T2_{\rm ex}$, $\Delta\theta_{\rm ex}$ and $\Delta\phi_{\rm ex}$ (see [1] for definition) by fixed values close to 1.25 when computing $\chi^2_{\rm ex}$. When these quantities are used to compute $\chi^2_{\rm muc}$, they are left unchanged. The scaling factors have been derived by comparing the widths of the pull distributions $(T_{\rm ex} - T_{\rm fit})/\sigma_T$ (where T stands for x, y, θ and ϕ coordinates) obtained for real and MC data. One can see in figure 7 the better agreement obtained between real and MC data for the $\chi^2_{\rm ex}/\chi^2_{\rm global}$ ratio after the $\chi^2_{\rm ex}$ scaling. It is performed inside MUCFIX when ISTEER(25)=1. The values of the scaling factors are contained in the variables SMFT1EX, SMFT2EX, SMFTHEX and SMFPHEX.

To obtain good agreement between real and MC data, it is also important to tune correctly the layer efficiencies implemented in the MC in order to reproduce the number of associated layers observed in the real data. The layer efficiencies are determined separately in each End Cap for the Very Loose tag and the 3 others, based on the same refit conditions. They are shown in table 5. The lower efficiencies obtained for the refits other than the Very Loose one come from the tighter cut applied on $\chi^2_{\rm bad\ hit}$. The efficiencies obtained in End Cap C are lower than in End Cap A because of some problems affecting the LTD's used to read the drift times in C. These problems only affected the last half of 1993 data taking, while they were present for the full 1994 data taking periods. A modification of the algorithm used inside DELANA to reconstruct the impact points detected in the forward muon chambers is currently under investigation. This modification could allow the recovery of most of the lost hits in End Cap C, and to reduce the efficiency difference between the two End Caps. The $N_{\rm layer}$ distributions obtained for muon pairs with the tuned layer efficiencies are shown in figure 8 in case of standard refit conditions. Good data MC agreement is observed.

The $\chi^2_{\rm global}$ p.d.f. and $\chi^2_{\rm ex}$ p.d.f. distributions obtains after the fixings are shown in figure 9 for the various muon samples. Good agreement between real and MC data is obtained for these χ^2 distributions. The small disagreements observed for small $\chi^2_{\rm global}$ values do not affect the tagging performance as no tag uses a cut lower than 2 on $\chi^2_{\rm global}$.

Table 5: MUF layer efficiencies

	Very Loose Refit		Other Refits	
Year	End Cap A	End Cap C	End Cap A	End Cap C
1993	92.4 ± 0.4 %	89.3 ± 0.4 %	86.6 ± 0.5 %	85.0 ± 0.5 %
1994	93.4 ± 0.3 %	86.7 ± 0.3 %	88.1 ± 0.3 %	82.2 ± 0.4 %

5 Improvements in the Barrel Region

The z coordinate in MUB is measured by delay line techniques: it is determined from the difference in times of arrival of the signals at the two ends of the chamber. For each of the 1372 chambers a calibration is required for the signal propagation velocity; this velocity is parametrised as a fifth order polynomial. The calibration of these chambers was performed in Oxford prior to installation. The present MUB configuration in DELPHI, however, contains certain chambers which were not calibrated, chambers which are now known to have been wrongly calibrated, and chambers whose delay line properties seem to have changed with time. Consequently the z resolution is rather poor, as can be seen from figure 10, which shows the difference between the reconstructed coordinate and the extrapolated track in muon pair events. This has been fitted with a single Gaussian of width 2.67 cm, but there are significant tails which make the effective resolution considerably worse. It is these tails in particular which until now have made z an unsafe variable to include in the MUFLAG tag association; rather, the emphasis has been placed on $R\phi$ (see section 2).

In addition to poor chamber to chamber calibration, there exists a systematic offset in z of the reconstructed hit to the track extrapolation. This varies in z and is largest at $|z| = 370$ cm, where it reaches 4 cm. It is not understood whether the problem arises in the track reconstruction or within the muon chambers. Hitherto, to overcome this problem in the association, an empirically determined correction to the extrapolation has been made prior to the fit (see [1]).

With the large statistics now available, it is possible to recalibrate the MUB delay lines from the data. This was done with the muon pairs collected in 1994, which gave around 150 hits per chamber. In the recalibration the systematic 'z-shift' was taken as a property of the chambers and the correction removed from the extrapolation. The result of this recalibration, as seen in figure 10, improves the resolution to 1.10 cm.

MUCFIX has been modified so that this re-calibration can be included in the muon tag algorithm. The calibration constants are read in from the file MUBCAL94.DAT and the re-calibration enabled through the switch ISTEER(26).

Also shown in figure 10 is the rms of the hit minus extrapolation distribution as a function of z. This is given for both the old and the new calibrations. Recall that MUB consists of two hemispheres, with one set of chambers at positive z and one set at negative z. It can be seen that the resolution is best at the ends of the chambers and degrades towards the ends. Unless the calibration is perfect, this is a natural property of the delay line reconstruction. Although this feature remains in the new calibration, the difference between the middle and ends of the chambers is much less pronounced than in the old calibration. It is this behaviour which is responsible for the sag in the muon identification

efficiency around $\theta = 90°$, particularly seen for the tight tag (see figure 16b). An option now exists within MUCFIX, activated by the switch ISTEER(27), to make the assigned delay line chamber error a parabolic function of z in order to even out the θ dependence of the fit.

MUFLAG has been retuned for the 94B data to take advantage of these improvements. Because z is now a good variable, the '$R\phi$ emphasis' of the algorithm has been dropped, and the cuts are now placed on the two variables $\chi^2_{\rm global}$ and $\chi^2_{\rm ex}$, as detailed in section 2. This tuning was used in the '94B2' short DST production. As will be seen, the result is an improved discrimination against background, and an efficiency without significant dependence on θ in the Barrel region.

In tuning the MC to match the data, a similar phenomenon was observed as found in the forward tagging, namely that the relative contributions of $\chi^2_{\rm muc}$ and $\chi^2_{\rm ex}$ to $\chi^2_{\rm global}$ are significantly different in the data and the MC, and this difference arises because the smearing applied to the hits in the MC is bigger than the resolution now achieved in the data (see section 4). As for MUF, this problem can be overcome by scaling the quantities $\Delta T1_{\rm ex}$, $\Delta T2_{\rm ex}$, $\Delta\theta_{\rm ex}$ and $\Delta\phi_{\rm ex}$ within the fit, and a good data MC agreement is possible for both $\chi^2_{\rm global}$ and $\chi^2_{\rm ex}$. Within MUCFIX this scaling is made when the switch ISTEER(28) is set, and the scaling factors are contained within the variables SMBT1X, SMBT2X, SMBTHX and SMBPHX.

The $\chi^2_{\rm global}$ p.d.f. and $\chi^2_{\rm ex}$ p.d.f. distributions obtained in MUB with these new 94B2 tunings are shown in figure 11.

Because the data are used to re-calibrate the chambers, there is a worry that these data cannot then be used to measure the efficiency of the algorithm, as the sample is now biased. In fact the correlation introduced has negligible effect. This was established by re-calibrating the chambers on only the even run numbers in the sample, and comparing the resolutions of the even and odd run numbers obtained with this calibration. No significant difference was observed.

6 Muon Identification Efficiencies

In this section, we present the muon identification efficiencies obtained with the three muon samples described in section 3. The efficiencies obtained for real and MC data are compared for the 4 possible muon tags. For the Barrel region, we will give results obtained with the 93C, 94B1 and 94B2 tunings. For the Forward region, we will only give the 93C and 94B1 results, the 94B1 and 94B2 results being identical.

Recall that only muons with a momentum greater than 3 GeV/c are considered. Their polar angle θ is also required to be inside the angular acceptance of MUB ($52.0° \leq \theta \leq 88.5°$ and $91.5° \leq \theta \leq 128.0°$) or MUF ($20.0° \leq \theta \leq 42.0°$ and $138.0° \leq \theta \leq 160.0°$).

6.1 Global efficiencies

The global muon identification efficiencies obtained for the various muon samples are shown in tables 6 to 10.

In the Barrel region (tables 6, 7 and 8), the efficiencies obtained with the Loose tag in the 93C and 94B1 data are generally larger for MC than for real data. This disagreement is reduced to less than 1 % in the 94B2 data. A better agreement between real and

MC data is obtained for the Very Loose, Standard and Tight tags. The results obtained for the 93C and 94B1 real and MC data are rather stable. In the tables 6 and 7, the efficiencies obtained from the various samples are compatible within errors, indicating the absence of momentum dependence. On the contrary, the 94B2 results show a rather strong momentum dependence. We will quantify more precisely this momentum dependence later on.

The results obtained in the Forward region (tables 9 and 10) show generally a good agreement between the real and MC data. All the results are compatible taking into account the statistical errors. They are almost identical between 93C and 94B processings. The ~ 3.5 % inefficiency of the Very Loose tag obtained for muon pairs comes from muons hitting the support cross of the MUF quadrants.

Table 6: Muon Identification Efficiencies in MUB for 93C Data

Data		Very Loose	Loose	Standard	Tight
$Z^0 \to \mu^+\mu^-$	Real	95.5 ± 0.2	90.9 ± 0.2	81.9 ± 0.3	67.7 ± 0.4
	MC	96.2 ± 0.1	95.1 ± 0.1	83.0 ± 0.2	70.1 ± 0.2
$\tau^- \to \mu^-\bar{\nu}_\mu\nu_\tau$	Real	95.2 ± 0.4	90.5 ± 0.5	82.3 ± 0.7	66.6 ± 0.9
	MC	96.0 ± 0.2	94.6 ± 0.2	82.2 ± 0.4	69.8 ± 0.5
$\gamma\gamma \to \mu^+\mu^-$	Real	93.0 ± 1.0	90.3 ± 1.2	83.0 ± 1.6	63.6 ± 2.3
	MC	93.4 ± 0.6	92.7 ± 0.6	78.4 ± 1.1	65.3 ± 1.4

Table 7: Muon Identification Efficiencies in MUB for 94B1 Data

Data		Very Loose	Loose	Standard	Tight
$Z^0 \to \mu^+\mu^-$	Real	95.7 ± 0.1	90.7 ± 0.1	81.5 ± 0.2	68.0 ± 0.3
	MC	96.2 ± 0.1	95.2 ± 0.1	82.5 ± 0.2	67.8 ± 0.2
$\tau^- \to \mu^-\bar{\nu}_\mu\nu_\tau$	Real	95.6 ± 0.2	90.6 ± 0.3	81.2 ± 0.5	65.1 ± 0.7
	MC	96.3 ± 0.2	95.5 ± 0.2	83.1 ± 0.4	69.5 ± 0.5
$\gamma\gamma \to \mu^+\mu^-$	Real	90.5 ± 1.0	87.8 ± 1.1	77.5 ± 1.5	58.7 ± 2.1
	MC	94.1 ± 0.4	93.3 ± 0.4	77.1 ± 0.7	63.7 ± 0.9

Table 8: Muon Identification Efficiencies in MUB for 94B2 Data

Data		Very Loose	Loose	Standard	Tight
$Z^0 \to \mu^+\mu^-$	Real	95.7 ± 0.1	94.4 ± 0.1	84.8 ± 0.2	75.6 ± 0.2
	MC	96.1 ± 0.1	95.5 ± 0.1	84.6 ± 0.1	75.2 ± 0.2
$\tau^- \to \mu^-\bar{\nu}_\mu\nu_\tau$	Real	95.6 ± 0.2	91.4 ± 0.3	79.9 ± 0.5	65.9 ± 0.6
	MC	96.3 ± 0.2	92.6 ± 0.3	79.7 ± 0.4	65.8 ± 0.6
$\gamma\gamma \to \mu^+\mu^-$	Real	90.6 ± 1.0	85.5 ± 1.2	69.1 ± 1.8	47.1 ± 2.4
	MC	93.3 ± 0.4	87.2 ± 0.5	66.9 ± 0.9	47.2 ± 1.1

Table 9: Muon Identification Efficiencies in MUF for 93C Data

Data		Very Loose	Loose	Standard	Tight
$Z^0 \to \mu^+\mu^-$	Real	96.3 ± 0.2	95.8 ± 0.2	90.0 ± 0.4	77.6 ± 0.6
	MC	96.4 ± 0.1	95.6 ± 0.1	90.0 ± 0.2	80.2 ± 0.3
$\tau^- \to \mu^-\bar{\nu}_\mu\nu_\tau$	Real	93.9 ± 0.6	91.8 ± 0.7	84.4 ± 1.0	66.5 ± 1.5
	MC	94.2 ± 0.4	92.4 ± 0.4	84.9 ± 0.6	69.4 ± 0.8
$\gamma\gamma \to \mu^+\mu^-$	Real	92.3 ± 0.6	90.5 ± 0.6	78.0 ± 1.0	54.8 ± 1.4
	MC	92.2 ± 0.3	90.3 ± 0.4	77.7 ± 0.6	53.7 ± 0.8

Table 10: Muon Identification Efficiencies in MUF for 94B1 Data

Data		Very Loose	Loose	Standard	Tight
$Z^0 \to \mu^+\mu^-$	Real	96.5 ± 0.2	95.9 ± 0.2	89.6 ± 0.3	77.1 ± 0.4
	MC	96.5 ± 0.1	95.9 ± 0.1	89.6 ± 0.2	77.9 ± 0.3
$\tau^- \to \mu^-\bar{\nu}_\mu\nu_\tau$	Real	94.4 ± 0.4	92.4 ± 0.5	84.5 ± 0.7	67.9 ± 1.0
	MC	94.0 ± 0.4	92.5 ± 0.4	83.8 ± 0.6	67.7 ± 0.9
$\gamma\gamma \to \mu^+\mu^-$	Real	92.2 ± 0.5	90.2 ± 0.6	77.3 ± 0.9	54.7 ± 1.2
	MC	92.2 ± 0.2	90.7 ± 0.3	78.1 ± 0.4	55.8 ± 0.6

6.2 Momentum Dependence

Comparing the efficiencies obtained in the Forward region between the various muon samples, a momentum dependence is clearly visible. This is demonstrated in figure 12 that shows the Standard tag efficiency in function of muon momentum for the three muon samples. The efficiency obtained for muons coming from two photons collisions is also lower that the one obtained from $\tau^- \to \mu^-\bar{\nu}_\mu\nu_\tau$ events in same momentum range. This effect is well reproduced by the MC data. It is related to the difference between the momentum spectrum of these two kinds of muons, those corresponding to $\gamma\gamma \to \mu^+\mu^-$ events being strongly peaked to small values (see figure 2). Close to 3 GeV/c, the intrinsic limit on the muon identification, efficiency starts to fall rapidly because of range out and severe multiple scattering in the iron.

To study the momentum dependence of muon identification efficiency, we use only muons produced in $Z^0 \to \mu^+\mu^-$ and $\tau^- \to \mu^-\bar{\nu}_\mu\nu_\tau$ events. Merging these two data sets, we apply a linear fit on the efficiency ϵ_μ versus muon momentum P_μ of the type :

$$\epsilon_\mu = a_0 + a_1 P_\mu \tag{11}$$

The tables 11 and 12 shows the values of the fitted parameter a_1 (expressed in %/GeV) obtained in the Forward and Barrel region respectively.

In the Forward region, the momentum dependence is already noticeable for the Very Loose tag and increase strongly when using tighter tags. The a_1 parameter reach ~ 0.16 %/GeV for the Standard tag, i.e. a ~ 7 % efficiency difference between 3 and 45 GeV/c muons. Nevertheless, these slopes are rather well reproduced by the MC data for the 4 tags. The main origin of this momentum dependence is to be found in the use of the extrapolation χ^2. Comparing the $\chi^2_{\rm ex}$ p.d.f. distributions obtained for the various muon

samples (figures 9b, 9d and 9f), one clearly sees that χ^2_{ex} becomes larger as the muon momentum decreases, while the applied cut for a given tag remains unchanged.

Table 11: Muon Momentum dependence in MUF (in %/GeV)

Data	Year	Very Loose	Loose	Standard	Tight
Real	93C	0.05 ± 0.02	0.12 ± 0.03	0.17 ± 0.04	0.35 ± 0.06
	94B	0.06 ± 0.02	0.11 ± 0.02	0.16 ± 0.03	0.29 ± 0.04
MC	93C	0.06 ± 0.01	0.09 ± 0.01	0.15 ± 0.02	0.26 ± 0.03
	94B	0.07 ± 0.01	0.10 ± 0.01	0.17 ± 0.02	0.29 ± 0.03

In the Barrel region, this parameter remains compatible with zero for 93C and 94B1 data, except for the Tight tag applied on the 94B1 real data. This is no more the case with 94B2 tuning because of the modification of the tagging criteria. Nevertheless, we obtain similar slopes between real and MC data. The reason for this dependence is the same as in the Forward region.

Table 12: Muon Momentum dependence in MUB (in %/GeV)

Data	Year	Very Loose	Loose	Standard	Tight
Real	93C	0.02 ± 0.02	0.01 ± 0.02	-0.03 ± 0.03	0.06 ± 0.04
	94B1	0.01 ± 0.01	< 0.01	< 0.01	0.12 ± 0.03
	94B2	0.01 ± 0.01	0.11 ± 0.01	0.20 ± 0.02	0.39 ± 0.03
MC	93C	< 0.01	< 0.01	0.03 ± 0.02	0.02 ± 0.02
	94B1	< 0.01	< 0.01	< 0.01	-0.05 ± 0.02
	94B2	< 0.01	0.10 ± 0.01	0.18 ± 0.02	0.35 ± 0.02

Although the cause of this momentum dependence is understood and is well reproduced in the MC, it is conceivable that certain analyses might require a flatter response with momentum. This can be obtained by merely altering the cuts on χ^2_{global} and χ^2_{ex}, quantities which are written to the short DST.

The figures 13 and 14 show the four tags efficiency in function of momentum obtained in the Barrel region with the 94B1 and 94B2 tuning respectively. The fit results are also represented. The figure 15 shows the results obtained in the Forward region for the 94B1 data. Good agreement between data and MC is obtained for each tag.

6.3 Polar Angle Dependence

The muon identification efficiency dependence on the polar angle is shown in figure 16. These efficiencies are obtained by combining muons coming from $Z^0 \rightarrow \mu^+\mu^-$ events and from τ decays. The 94B1 results for the Standard and Tight tags are shown on figures 16a and 16b respectively. The 94B2 results are shown on figures 16c and 16d.

In the Forward region, small discrepancies between real data and MC are observed in one End Cap ($\theta \leq 42.0°$). Their are related to the problem affecting the End Cap C LTD's discussed previously (see section 4).

In the Barrel region, the discrepancies observed in the $\theta \sim 90°$ region for 94B1 results are related to badly measured coordinates at the edge of the barrel muon chambers. The new calibration of the MUB delay line velocities and the scaling of the assigned errors with chamber position cure the efficiency drop in this region, as demonstrated in figure 16d.

7 Muon Misidentification Probabilities

The $\tau^- \to \pi^-\pi^-\pi^+\nu_\tau$ events are used to determine the muon misidentification probability for the 4 muon tags. The results presented in this section have been corrected for the contamination of these pion samples by others particles.

The table 13 shows the misidentification probabilities obtained from these data samples in the Barrel region. For the Very Loose tag, the misidentification probability is clearly larger on the real data than on the MC. For the other tags, reasonable agreement between real and MC data results is observed taking into account the errors. Nevertheless, the real data results are systematicaly above the MC ones, the difference being at the level of 2σ. One obtains similar results between 93C and 94B1 data. For the 94B2 data, the misidentification probabilities obtained for the Standard and Tight tags are clearly improved, thanks to the better z resolution.

Table 13: Misidentification Probabilities in MUB (in %)

Data	Year	Very Loose	Loose	Standard	Tight
Real	93C	5.20 ± 0.29	1.23 ± 0.14	0.72 ± 0.11	0.49 ± 0.09
	94B1	4.94 ± 0.20	1.34 ± 0.11	0.80 ± 0.08	0.55 ± 0.07
	94B2	4.94 ± 0.20	1.31 ± 0.10	0.65 ± 0.07	0.42 ± 0.06
MC	93C	3.14 ± 0.13	1.09 ± 0.08	0.55 ± 0.05	0.36 ± 0.04
	94B1	2.89 ± 0.12	1.00 ± 0.07	0.52 ± 0.05	0.29 ± 0.04
	94B2	2.87 ± 0.12	0.66 ± 0.06	0.27 ± 0.04	0.16 ± 0.03

The misidentification probabilities obtained in the Forward region are shown in the table 14. One observes similar features to the ones described previously for the Barrel region, i.e. :

- Strong difference between the results obtained with real and MC data for the Very Loose tag. A closer look shows that this effect comes mainly from the difference between data and MC in the number of pion candidates with only one associated hit in MUF. In figure 17 are shown the N_{layer} distributions obtained in MUB and MUF for the 94B1 pion samples. The real and MC data distributions are normalised so as to correspond to the same number of π candidates. In the MUF, the number of π with one associated hit is almost twice as large in the real data than in the MC, while the number of π with $N_{layer} \geq 2$ is similar. This effect is probably related to an underestimation of π punch–through in MC. The situation is less evident in the MUB (figures 17a and 17c) but, again, the disagreement between data and MC comes mainly from pions with a small number of associated layers.

- The misidentification probability obtained with the Loose tag is reduced by more than a factor 3 with respect to the Very Loose tag. This Loose tag is thus a good

alternative to the Very Loose tag for physics analysis requiring a very high efficiency but having to deal with a large pion contamination (as for example in the study of the $\tau^- \to \mu^- \bar{\nu}_\mu \nu_\tau$ decay). Looking back to table 10, the loss of efficiency is limited to $\sim 2\%$ by using Loose instead of Very Loose tag. Nevertheless, the difference between real and MC data results is around 2.5 σ.

- For the Standard and Tight tags, one obtains similar results to those in the Barrel region. Here again, the real data show a larger misidentification probability than the MC, the difference being of the order of 1σ.

Table 14: Misidentification Probabilities in MUF (in %)

Data	Year	Very Loose	Loose	Standard	Tight
Real	93C	9.61 ± 0.91	2.68 ± 0.48	0.78 ± 0.26	0.61 ± 0.23
	94B	7.88 ± 0.60	2.28 ± 0.32	0.87 ± 0.20	0.55 ± 0.16
MC	93C	6.00 ± 0.43	1.48 ± 0.21	0.58 ± 0.13	0.36 ± 0.10
	94B	6.17 ± 0.43	1.78 ± 0.23	0.66 ± 0.14	0.36 ± 0.10

These results are similar to the ones obtained in an other analysis using the 92D and 93B data and different pion samples [7].

The momentum dependence of the misidentification probability is shown in figure 18 for the Very Loose and Standard tags. For the Very Loose tag in the Barrel region (figure 18a), the misidentification probability has a tendancy to increase with momentum. This is also the case for the MC data in the Forward region but not for the real data (figure 18b). On the contrary, the misidentification probability for the Standard tag seems to decrease with increasing momentum in the Barrel (figure 18c), while the statistics available in the Forward region does not allow one to draw any conclusion (figure 18d).

8 Conclusions

Thanks to the large statistics of leptonic events available in the 1993 and 1994 DELPHI data, significant improvements in the muon chambers data reconstruction have been obtained. This results in an improvement of the muon chambers resolution both in the Barrel and the Forward regions. The MC data tuning have also been modified in order to take into account this improved resolution.

Various muon samples have been selected allowing to study the dependences of muon identification efficiency in momentum and polar angle. These muons allow the study of the full momentum range from 3 GeV/c up to 45 GeV/c. Good agreement between real and MC data efficiencies is obtained for the 4 muon tags, especially with the 94B2 processing. For this processing, real and MC data agree to the 1 % level.

A sample of charged pions coming from $\tau^- \to \pi^-\pi^-\pi^+\nu_\tau$ events has been used to study the misidentification probability of the 4 muon tags. It remains below the 1 % level for the Standard and Tight tags, both in the Barrel and the Forward region.

Acknowledgments

The authors wish to thank Peter Renton for his help in re-calibrating the MUB delay lines.

References

[1] "EMMASS Muon Identification within DELPHI"
N. Crosland, G. Wilkinson, P. Kluit, DELPHI 92-17 PHYS 157, February 1992.

[2] "MUFLAG: A Framework for Muon Identification"
H. De Boeck and G. Wilkinson, DELPHI 93-14 PHYS 263, April 1993.

[3] "MUCFIX : Refining the Muon Chamber Information on the DST"
G. Wilkinson and P. Collins, DELPHI 93-13 PHYS 262, February 1993.

[4] "A Selection for τ Lepton Studies"
F. Matorras, DELPHI 92-124 PHYS 225, September 1992.

[5] "τ lepton cross section and charge asymmetry using the DELPHI forward region"
J. MacNaughton, F. Mandl and J. Strauss, DELPHI 94-19 PHYS 356, February 1994.

[6] "La Détection des Muons dans l'Expérience DELPHI et son Rôle dans l'Etude de l'Interaction $e^+e^- \to \mu^+\mu^-$"
F. Stichelbaut, Ph.D. Thesis, ULB 1993.

[7] "Study of standard muon tag in a pion sample"
J.-D. Durand, DELPHI 95–65 PHYS 500, 24 July 1995.

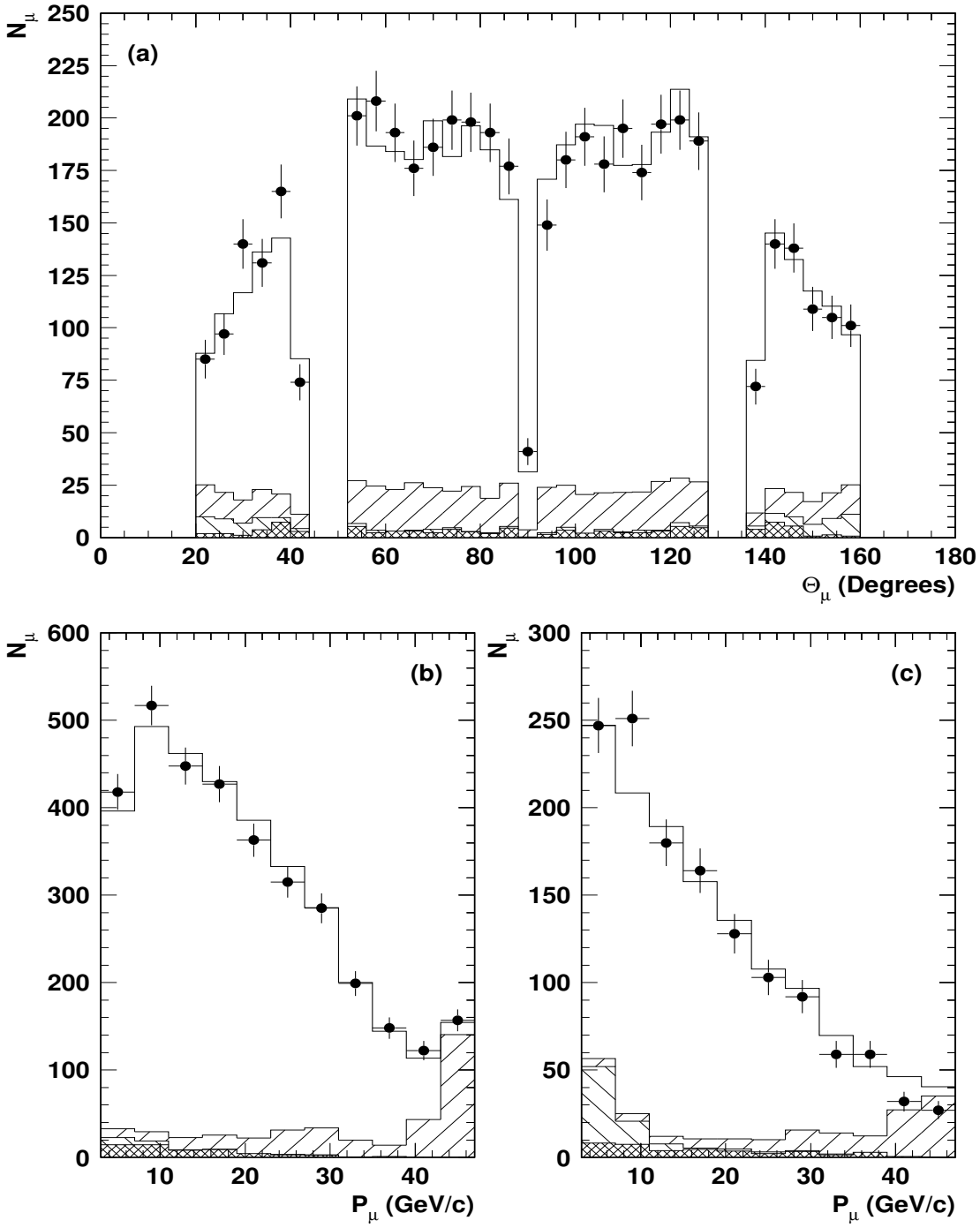

Figure 1: Kinematical properties of muon candidates coming from τ decays : polar angle distribution (a), momentum distribution in the Barrel region (b) and momentum distribution in the Forward region (c). The black dots correspond to the 93C real data. The double hatched histogram shows the background coming from τ's not decaying into a muon, the right hatched histogram shows the background coming from $Z^0 \to \mu^+\mu^-$ events and the left hatched shows the background from two photons collisions. The open histogram is the sum of these various backgrounds and the true signal.

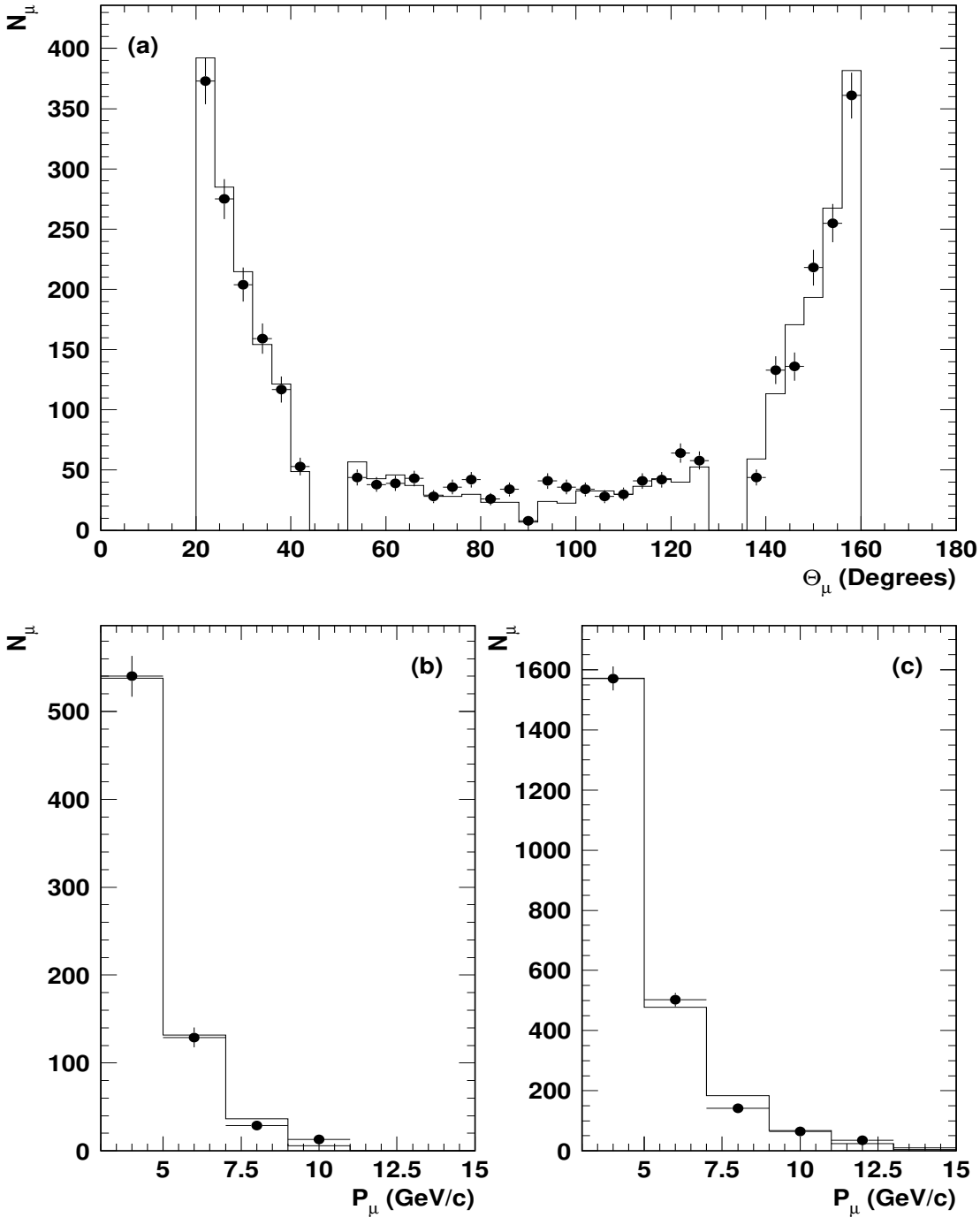

Figure 2: Kinematical properties of muon candidates coming from two photons collisions : polar angle distribution (a), momentum distribution in the Barrel region (b) and momentum distribution in the Forward region (c). The black dots correspond to the 93C real data. The histograms show the distributions obtained with MC data.

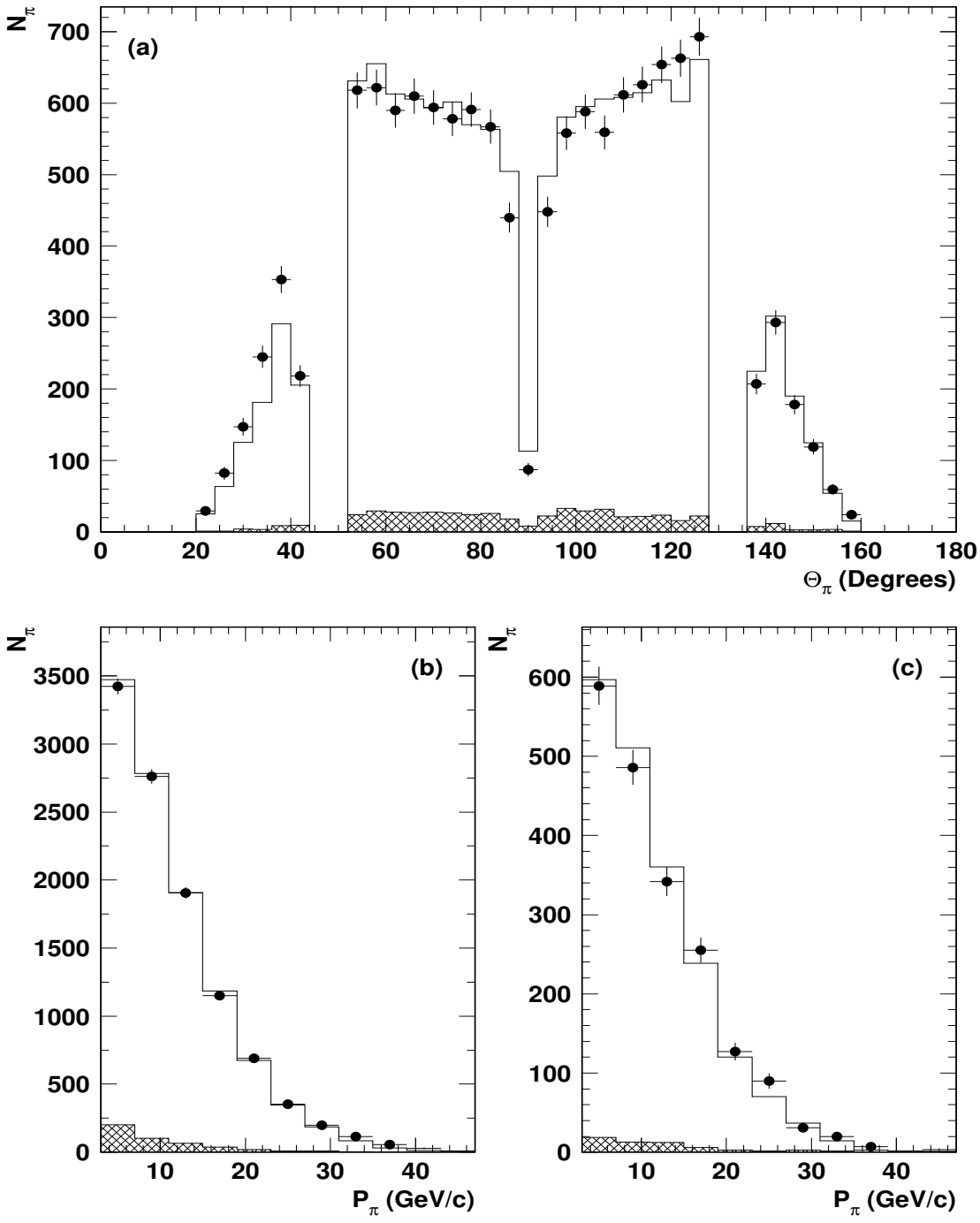

Figure 3: Kinematical properties of pion candidates coming from τ decays : polar angle distribution (a), momentum distribution in the Barrel region (b) and momentum distribution in the Forward region (c). The black dots correspond to the 94B real data. The open histograms show the distributions obtained from MC data. The double hatched histogram shows the background coming from τ's not decaying into three charged pions.

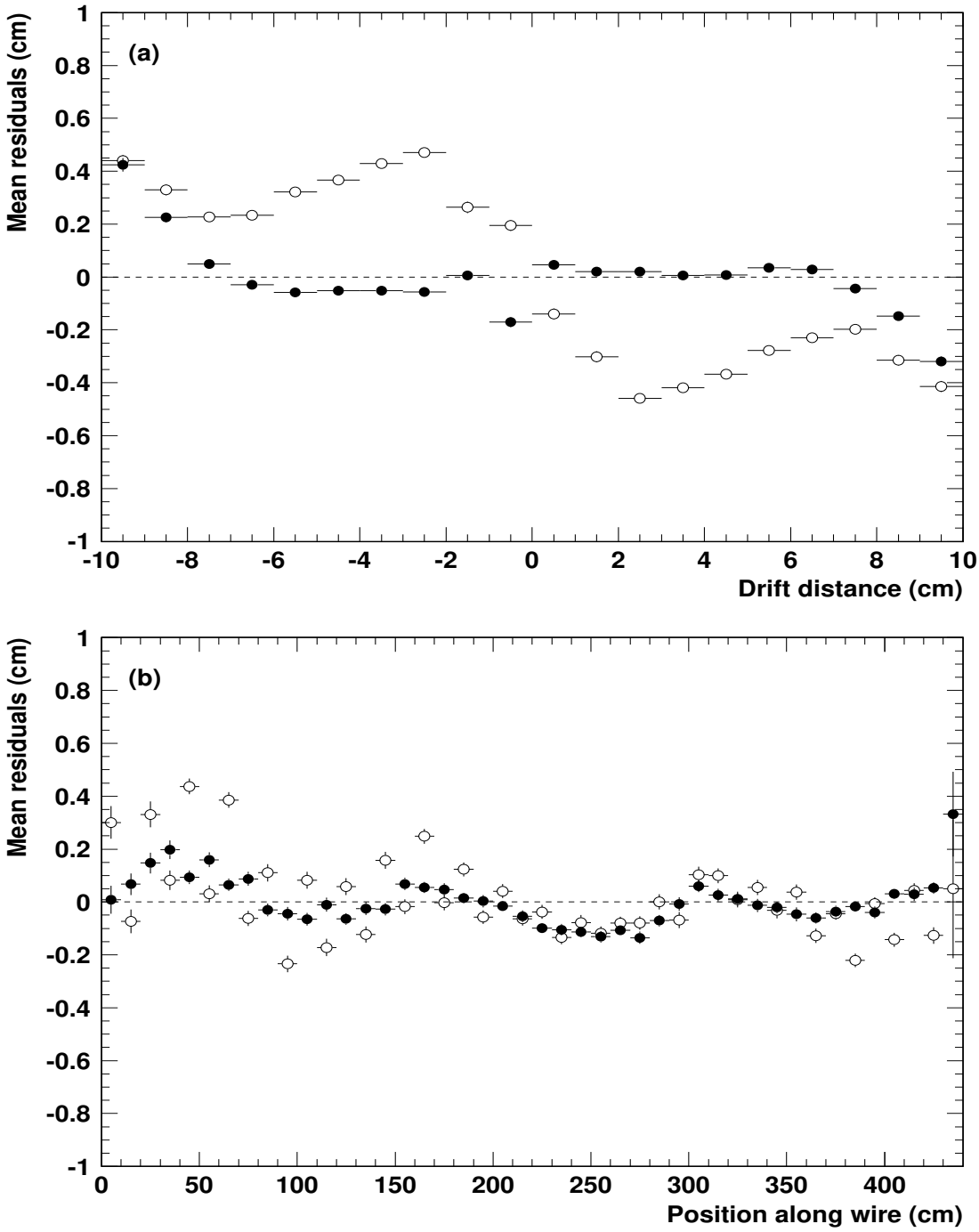

Figure 4: Mean residuals in function of the drift distance (a) and of the position along the anode wire (b). The open circles are residuals obtained before fixing and the solid circles shows the residuals after fixing.

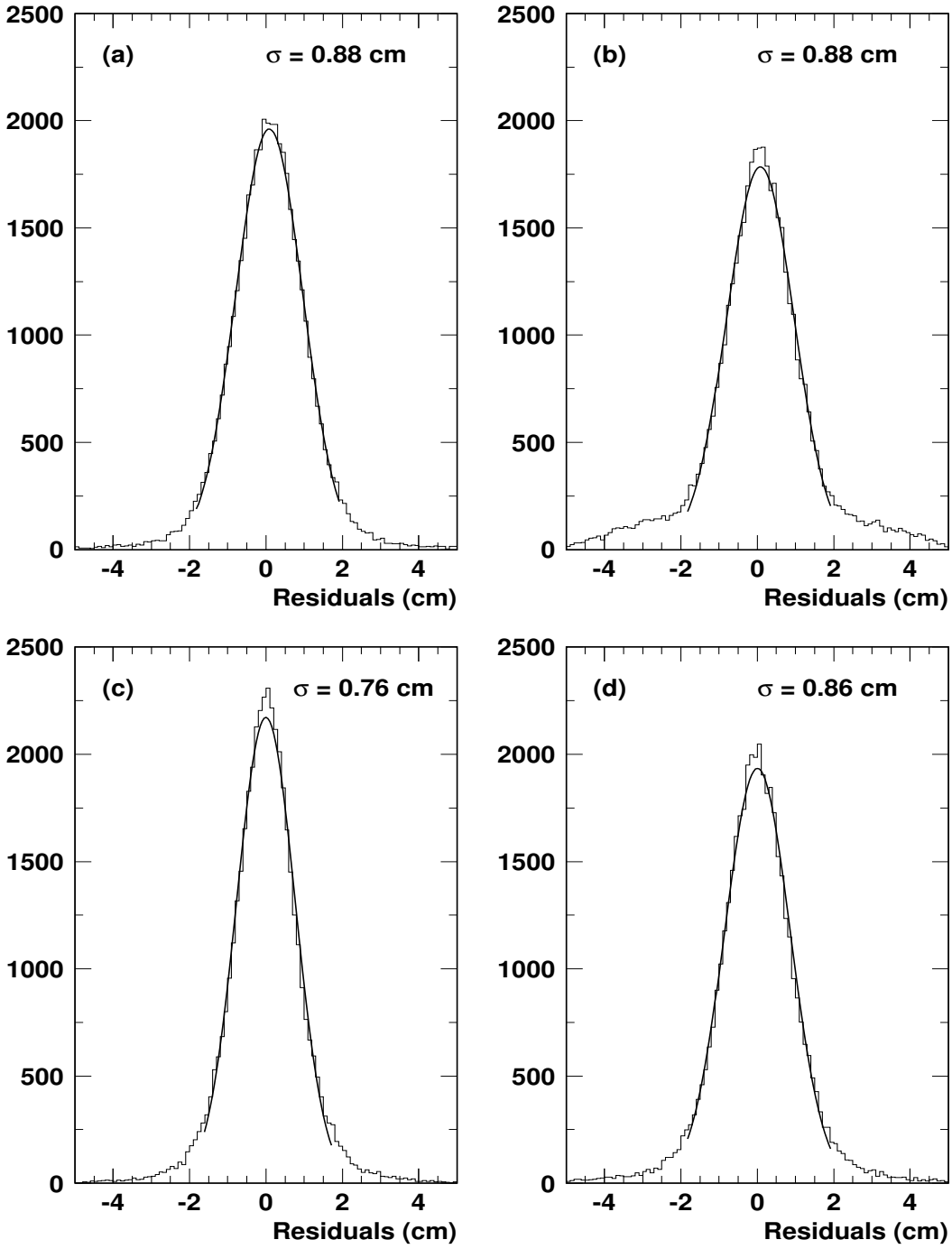

Figure 5: Distributions of residuals obtained for coordinates measured along the drift direction (a-c) and along the delay lines (b-d). The figures (a) and (b) correspond to the 93B data before any fixing while the figures (c) and (d) shows the residuals obtained after all fixings. The curves show the result of a Gaussian fit.

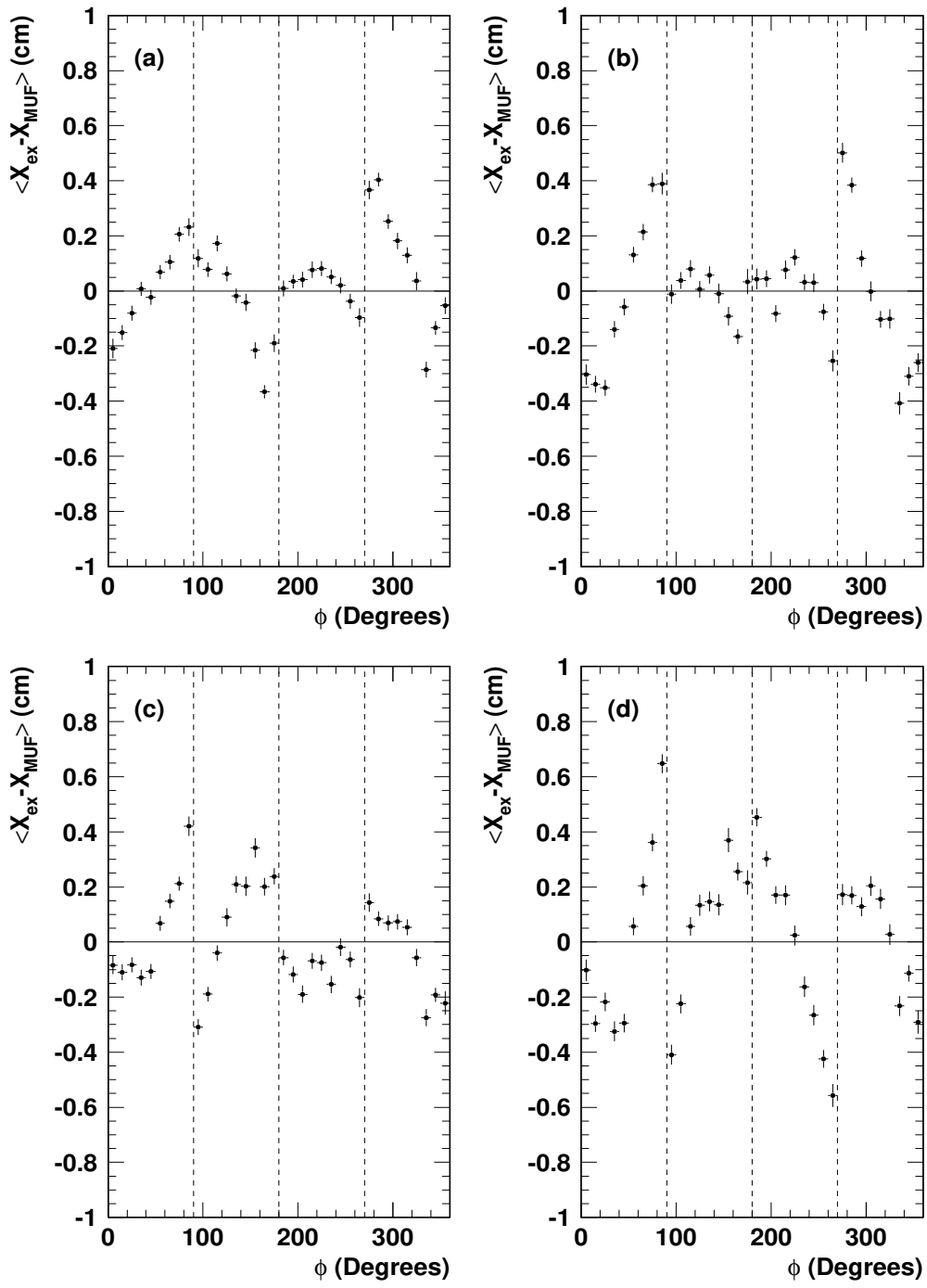

Figure 6: Evolution in function of ϕ of the systematic differences between extrapolated and measured coordinates in MUF along the DELPHI X axis. The four figures correspond to the 4 detection planes : inner (a) and outer plane (b) in End Cap A, inner (c) and outer plane (d) in End Cap C. These figures have been obtained with the 94B muon pairs data. The vertical dashed lines show the limits of the 4 quadrants inside a plane.

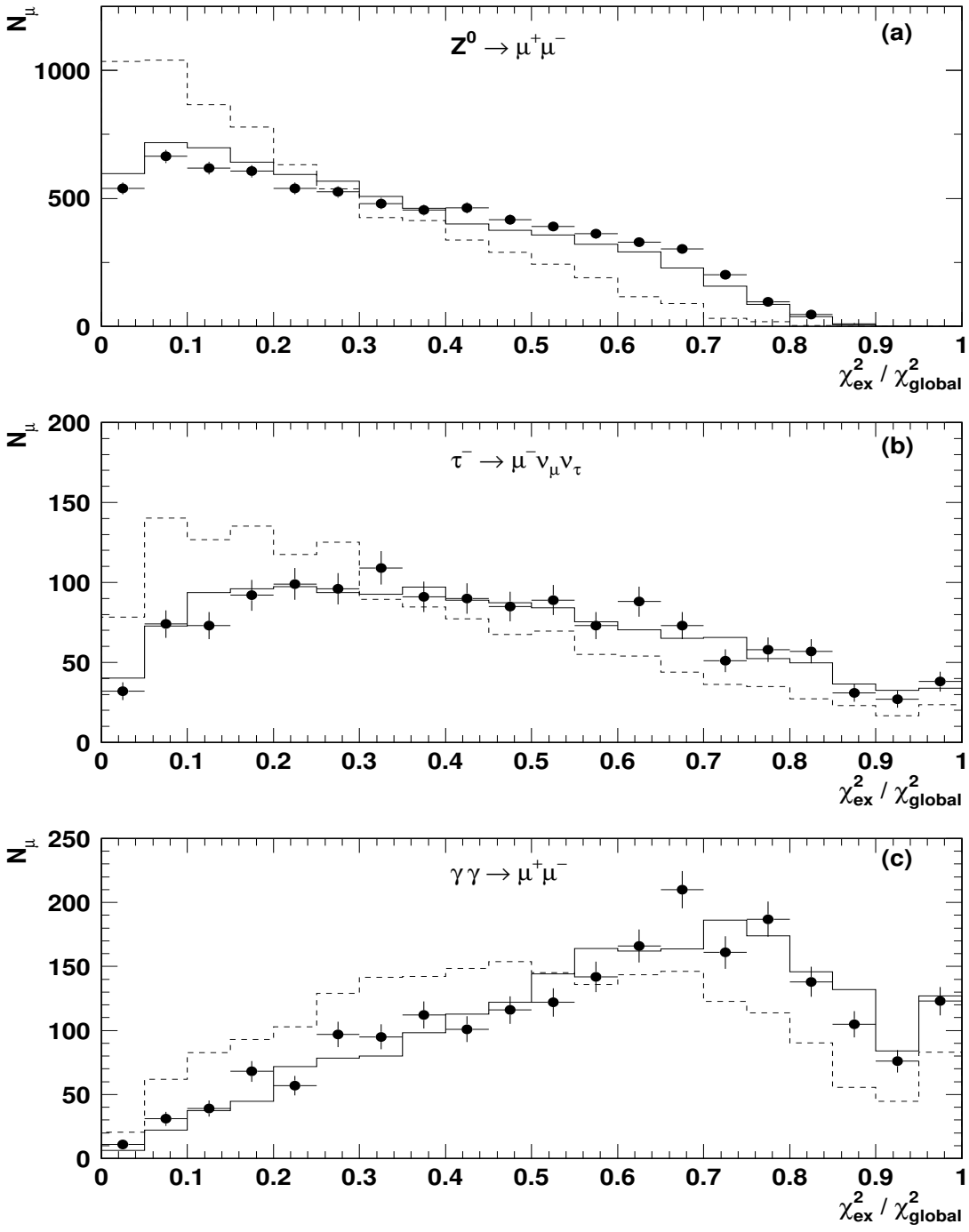

Figure 7: Ratio of extrapolation over global χ^2 for muons coming from $Z^0 \to \mu^+\mu^-$ (a), $\tau^- \to \mu^-\bar{\nu}_\mu\nu_\tau$ (b) and $\gamma\gamma \to \mu^+\mu^-$ events (c). The dots are the real data, the dashed and full lines are the MC data before and after rescaling respectively.

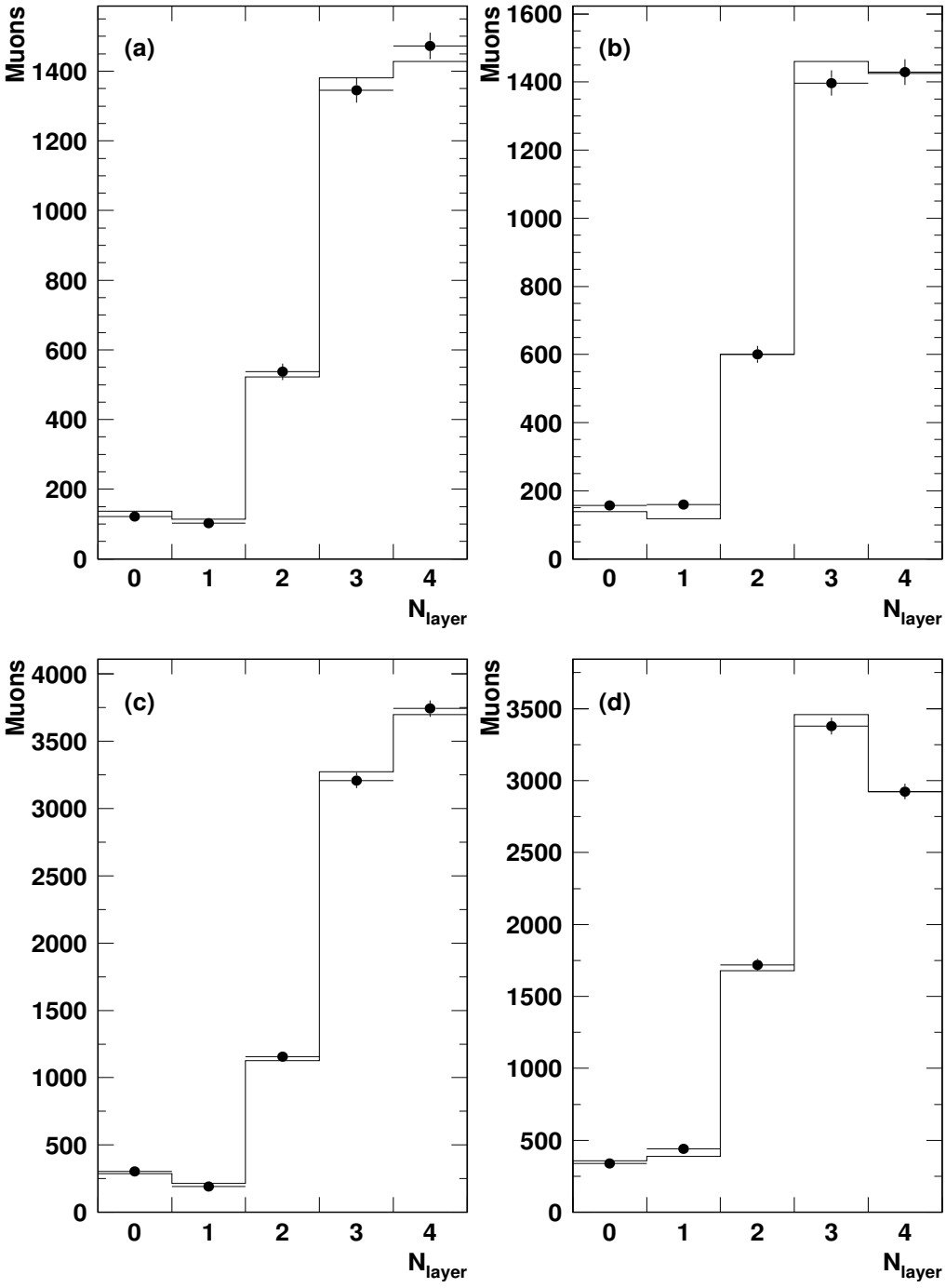

Figure 8: Distributions of the number of MUF layers associated to muon candidates coming from $Z^0 \rightarrow \mu^+\mu^-$ events for the standard refit. The dots correspond to the real data and the histograms to MC data. The distributions obtained in End Caps A and C with the 93C data are shown in figures (a) and (b) respectively. The distributions obtained with the 94B data are shown in figures (c) and (d).

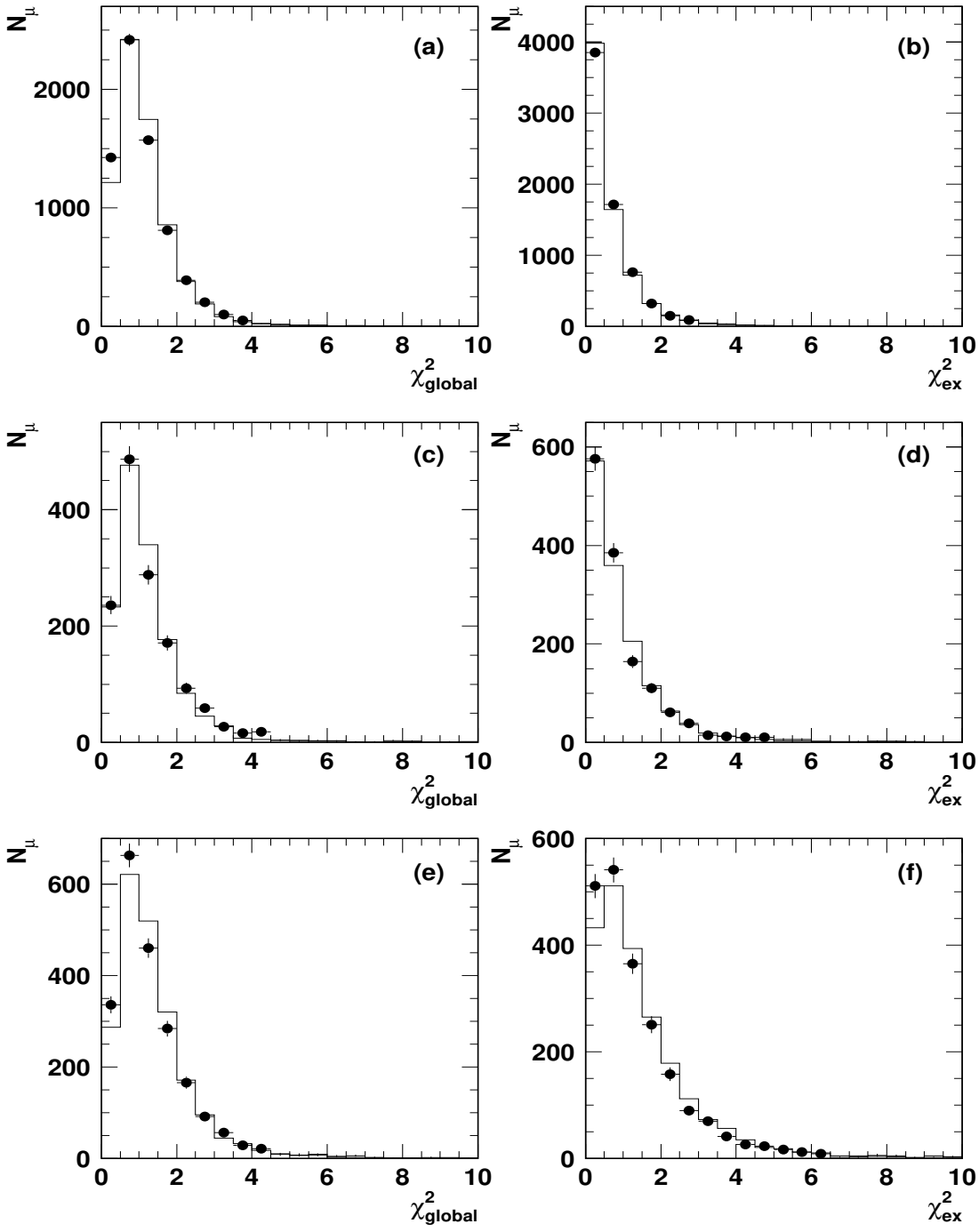

Figure 9: Distributions of $\chi^2_{\rm global}$ p.d.f. (a-c-e) and $\chi^2_{\rm ex}$ p.d.f. (b-d-f) obtained in the Forward region for the various muon samples : $Z^0 \to \mu^+\mu^-$ (a-b), $\tau^- \to \mu^-\bar{\nu}_\mu\nu_\tau$ (c-d) and $\gamma\gamma \to \mu^+\mu^-$ (e-f). The dots are the 93C real data and the histograms are the MC data.

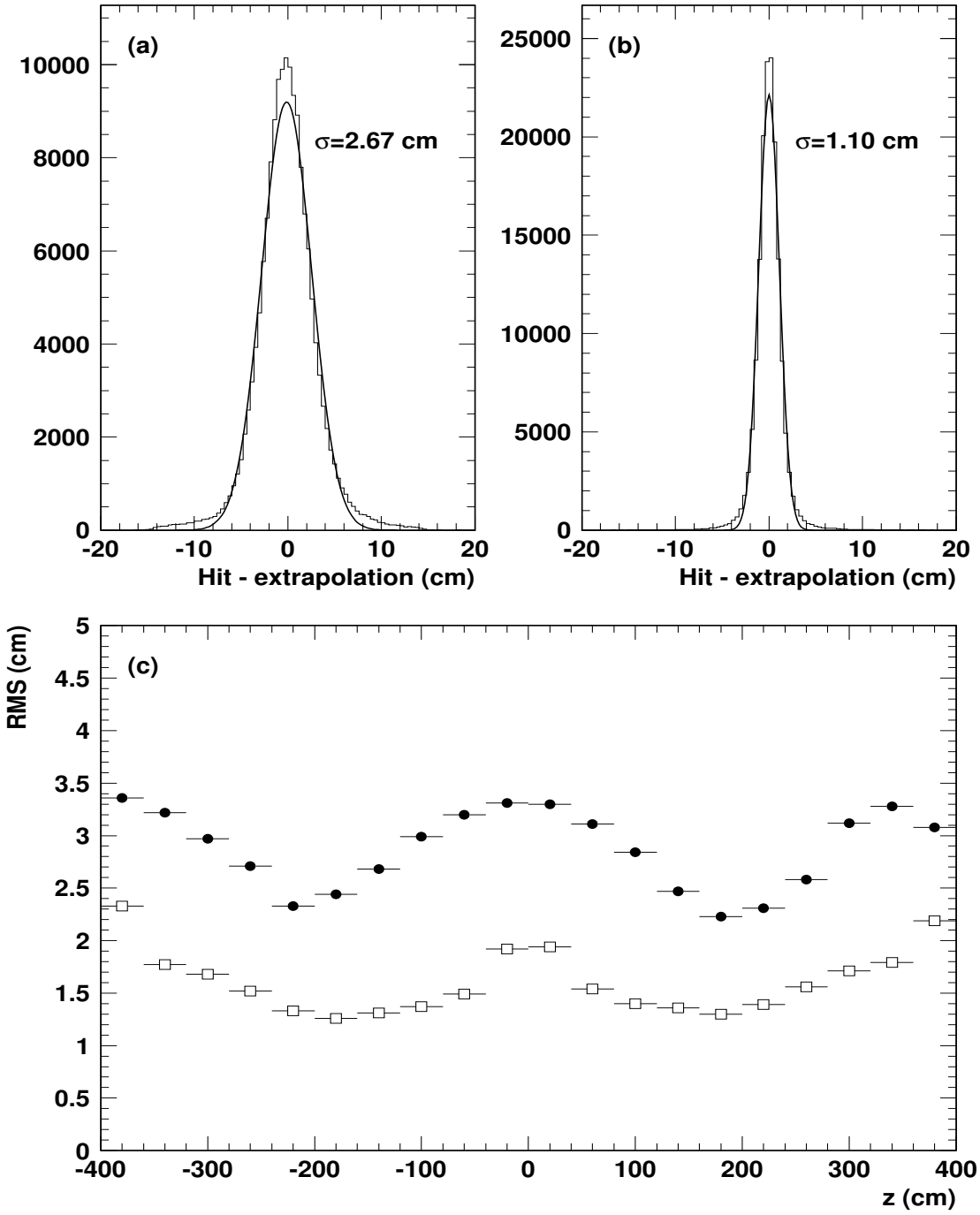

Figure 10: MUB z resolution before and after recalibration. (a) shows hit - extrapolation in z for muon pairs with old calibration; (b) shows the same distribution with the new calibration. In (c) is displayed the RMS of these two distributions as a function of z, with the old calibration the solid circles and the new calibration the open squares.

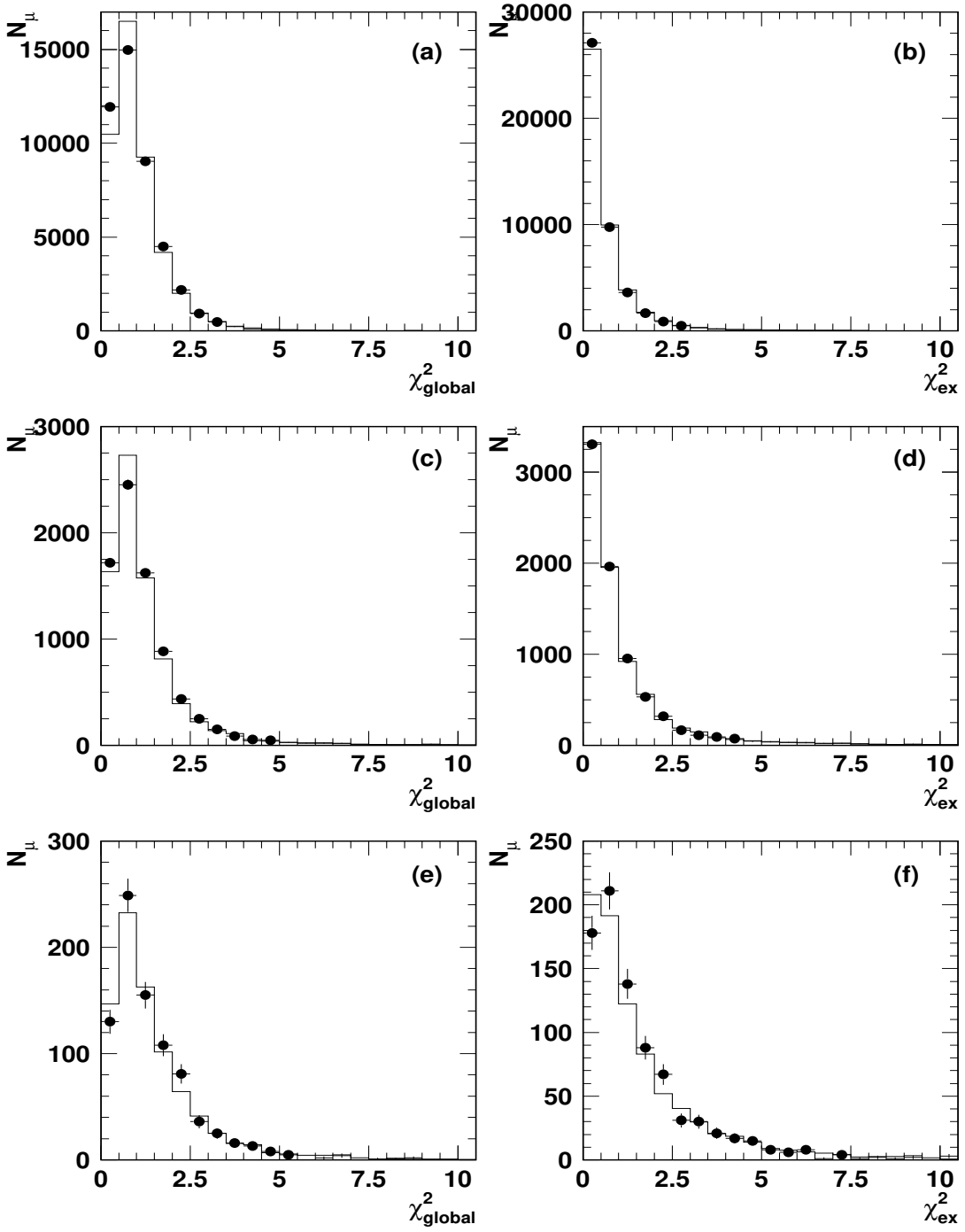

Figure 11: Distributions of $\chi^2_{\rm global}$ p.d.f. (a-c-e) and $\chi^2_{\rm ex}$ p.d.f. (b-d-f) obtained in the Barrel region for the various muon samples : $Z^0 \to \mu^+\mu^-$ (a-b), $\tau^- \to \mu^-\bar{\nu}_\mu\nu_\tau$ (c-d) and $\gamma\gamma \to \mu^+\mu^-$ (e-f). The dots are the 94B2 real data and the histograms are the MC data.

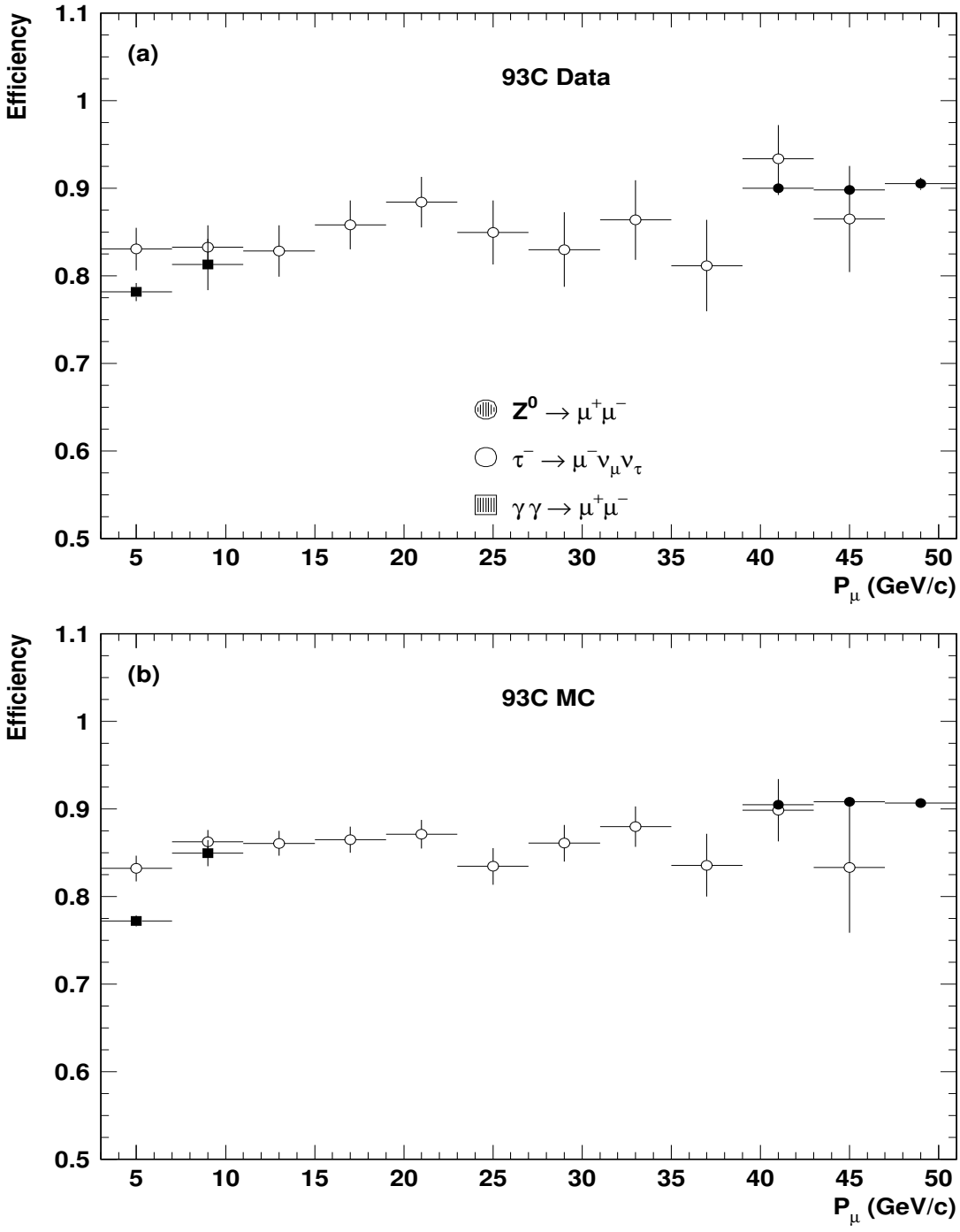

Figure 12: Identification efficiency in function of muon momentum for the Standard tag applied on real data (a) and on MC data (b).

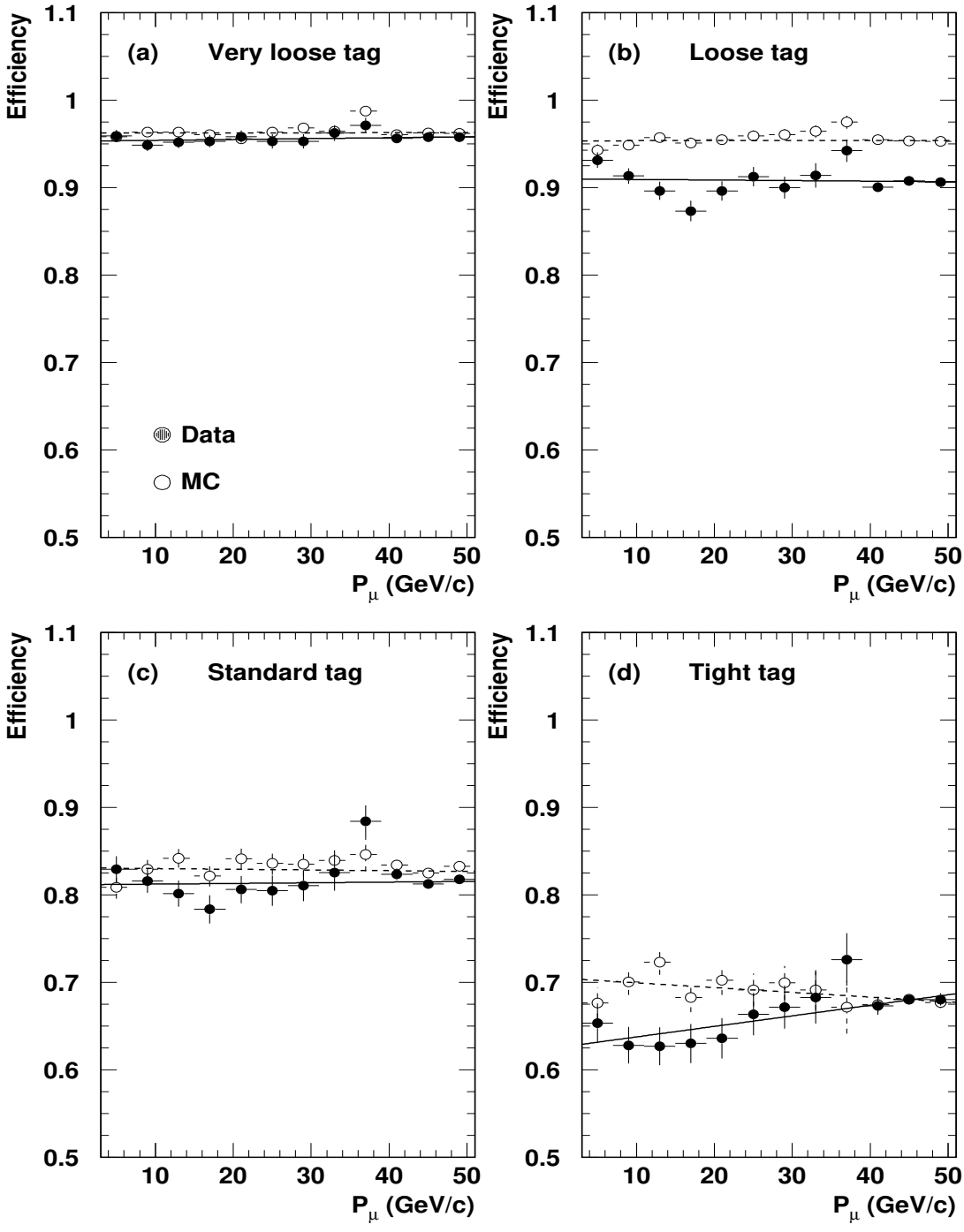

Figure 13: Muon identification efficiencies in function of momentum for the four muon tags in the Barrel. The 94B1 real data are represented by solid circles and the MC data by open circles. The full and dashed lines are the results of a linear fit applied to the real and MC data respectively (see text).

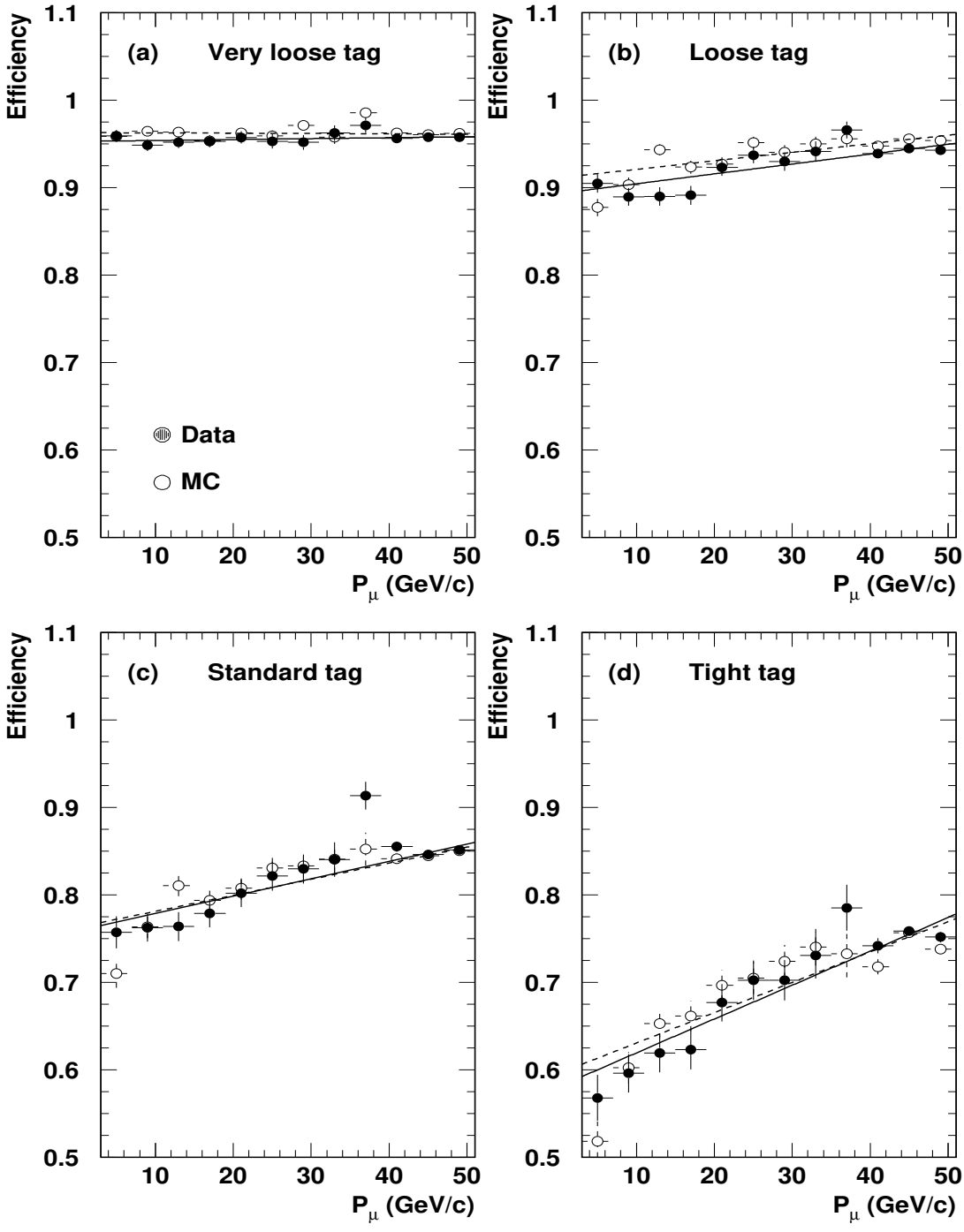

Figure 14: Muon identification efficiencies in function of momentum for the four muon tags in the Barrel. The 94B2 real data are represented by solid circles and the MC data by open circles. The full and dashed lines are the results of a linear fit applied to the real and MC data respectively (see text).

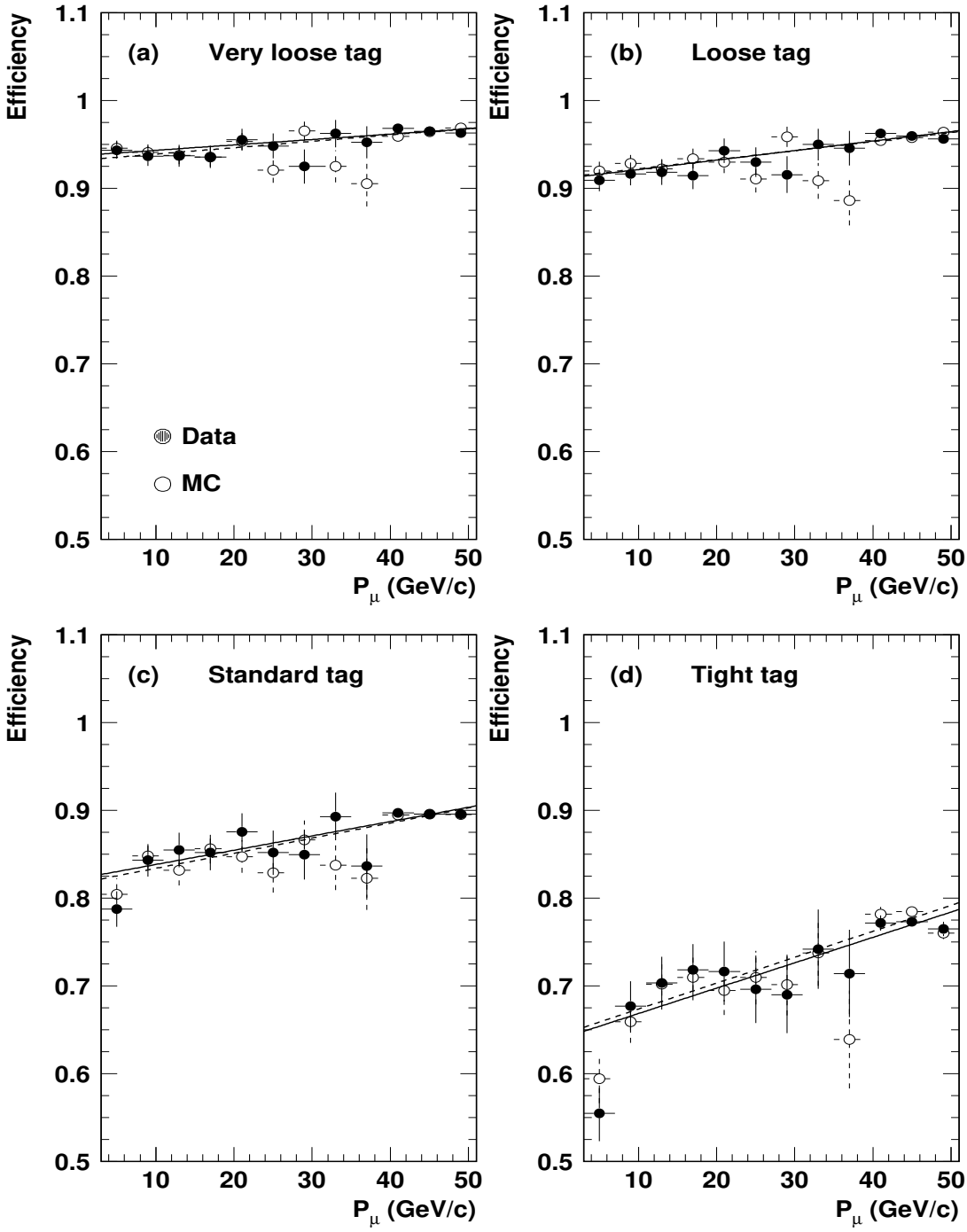

Figure 15: Muon identification efficiencies in function of momentum for the four muon tags in the Forward region. The 94B real data are represented by solid circles and the MC data by open circles. The full and dashed lines are the results of a linear fit applied to the real and MC data respectively (see text).

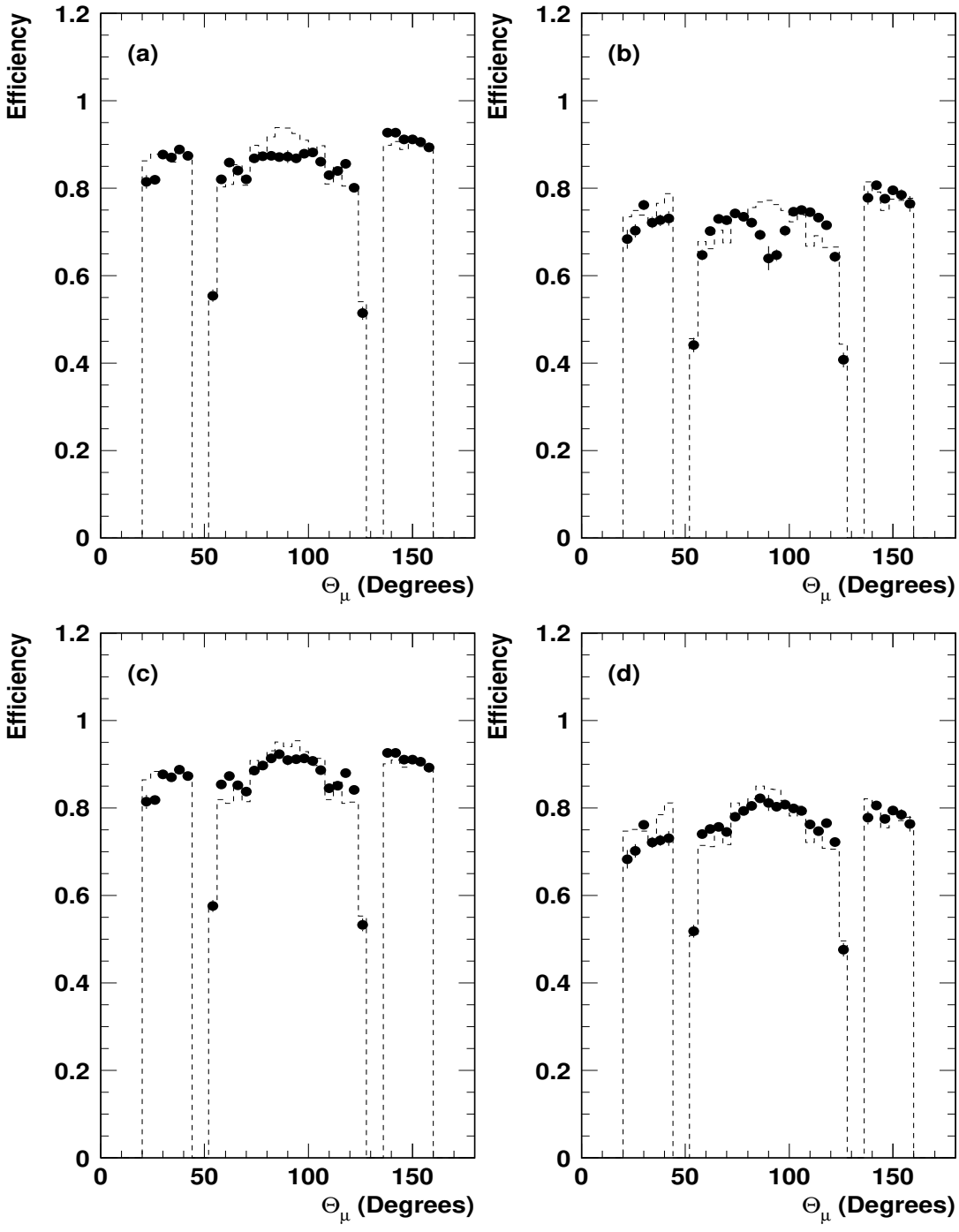

Figure 16: Muon identification efficiencies in function of polar angle for the Standard (a-c) and Tight (b-d) tags. The 94B1 results are shown in figures (a) and (b) while the 94B2 results are shown in figures (c) and (d). The real data are represented by the solid circles and the MC data by the dashed histograms.

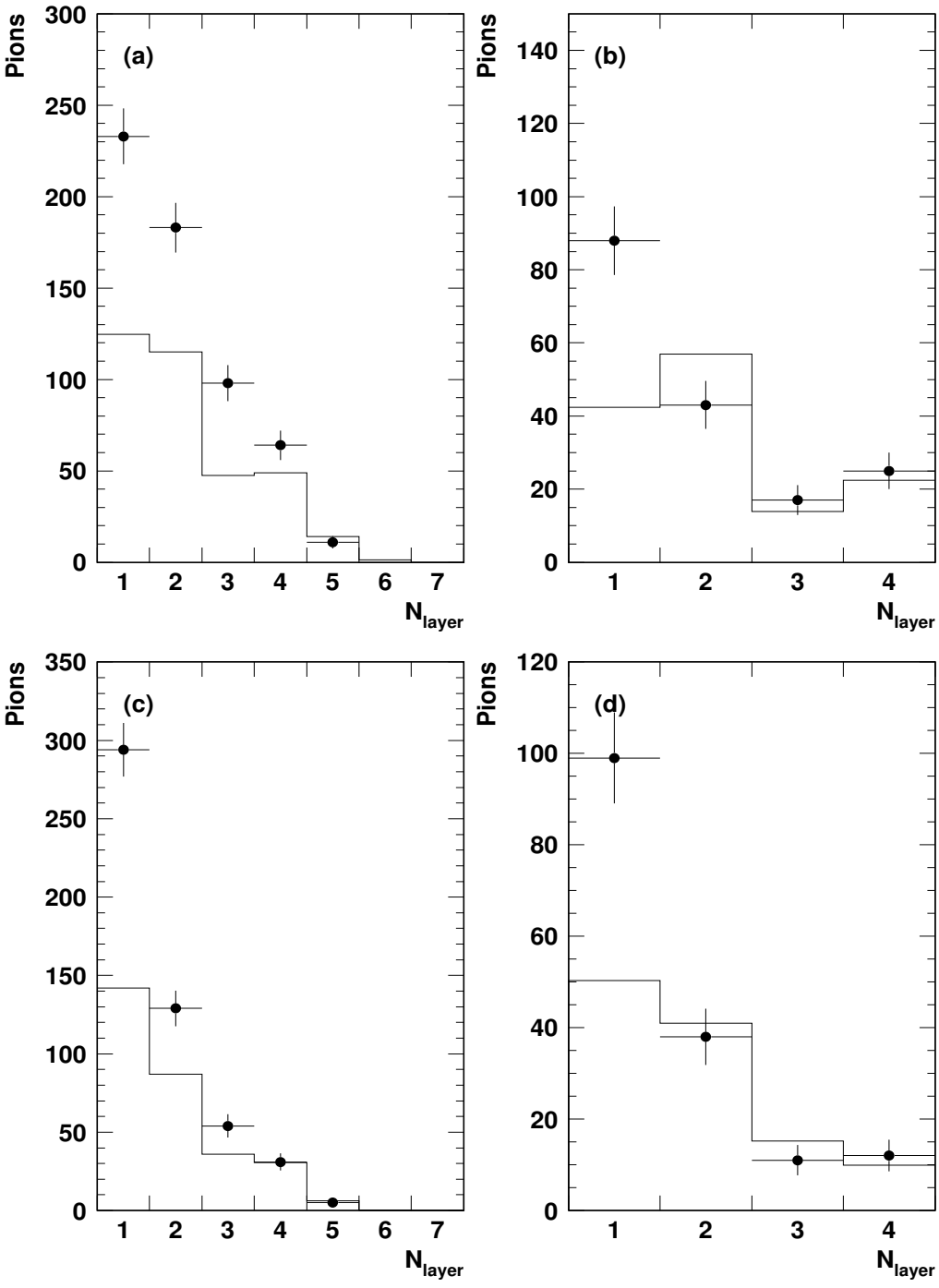

Figure 17: Distributions of the number of associated layers in MUB (a-c) and in MUF (b-d) for pions coming from 3–prong τ decays. The distributions (a-b) are obtained after the Very Loose refit and the distributions (c-d) after the standard refit. The dots represent the 94B1 real data and the histograms the MC data.

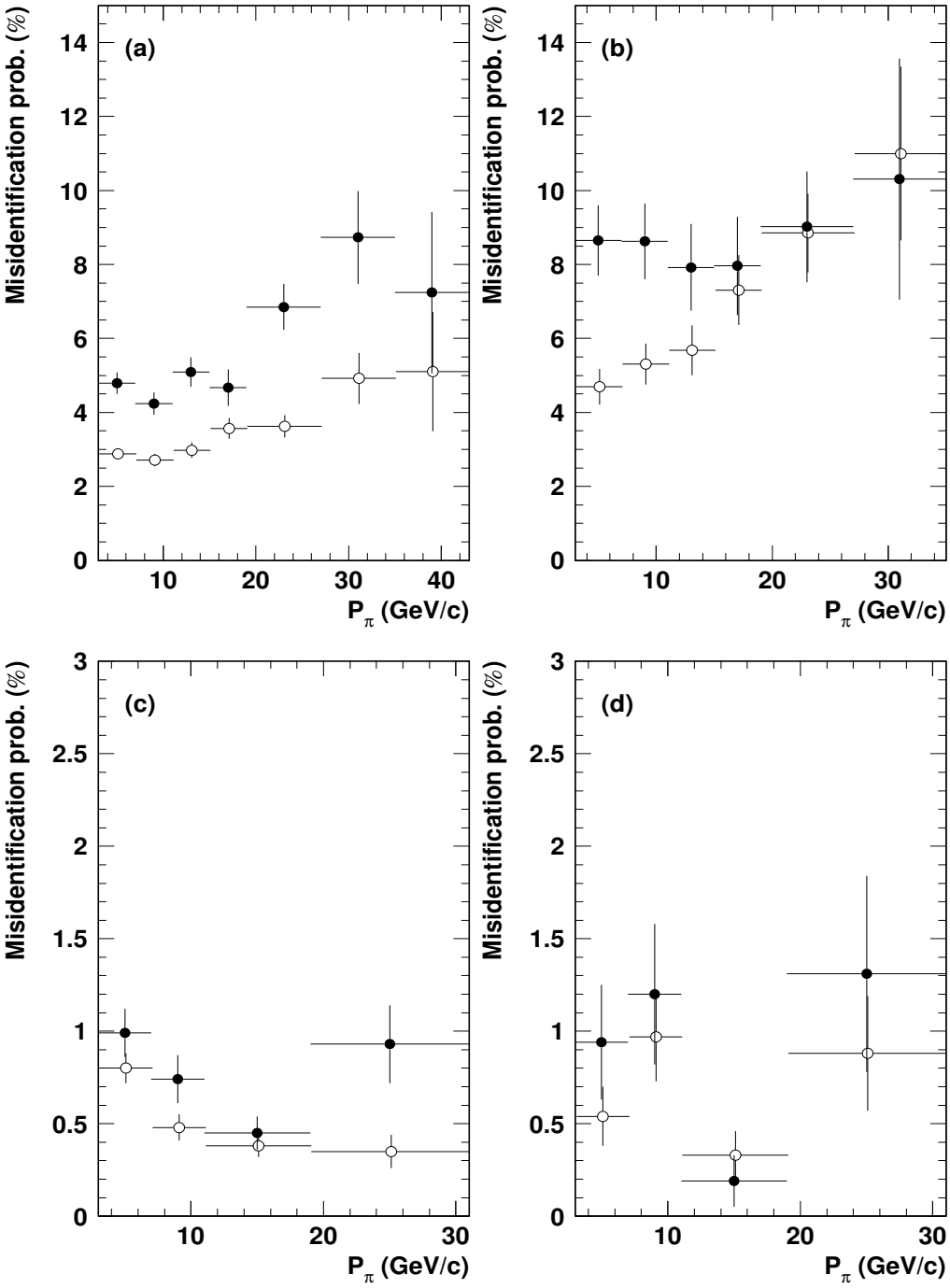

Figure 18: Evolution with pion momentum of the misidentification probabilities obtained with the Very Loose (a-b) and the Standard tag (c-d) respectively. The figures (a) and (c) correspond to the Barrel region while the figures (b) and (d) correspond to the Forward region. The closed circles are the real data adding 93C and 94B1 statistics, the open circles are the MC data.